

1 SEARCH FOR PRODUCTION OF A HIGGS BOSON AND A SINGLE TOP
2 QUARK IN MULTILEPTON FINAL STATES IN pp COLLISIONS AT $\sqrt{s} = 13$
3 TeV.

4 by

5 Jose Andres Monroy MontaÑez

6 A DISSERTATION

7 Presented to the Faculty of

8 The Graduate College at the University of Nebraska

In Partial Fulfilment of Requirements

10 For the Degree of Doctor of Philosophy

11 Major: Physics and Astronomy

12 Under the Supervision of Kenneth Bloom and Aaron Dominguez

13 Lincoln, Nebraska

14 July, 2018

15 SEARCH FOR PRODUCTION OF A HIGGS BOSON AND A SINGLE TOP
16 QUARK IN MULTILEPTON FINAL STATES IN pp COLLISIONS AT $\sqrt{s} = 13$
17 TeV.

18 Jose Andres Monroy Montañez, Ph.D.

19 University of Nebraska, 2018

20 Adviser: Kenneth Bloom and Aaron Dominguez

²¹ Table of Contents

²²	Table of Contents	iii
²³	List of Figures	vi
²⁴	List of Tables	viii
²⁵	1 INTRODUCTION	1
²⁶	2 Theoretical approach	2
²⁷	2.1 Introduction	2
²⁸	2.2 Standard model of particle physics	5
²⁹	2.2.1 Fermions	7
³⁰	2.2.1.1 Leptons	8
³¹	2.2.1.2 Quarks	10
³²	2.2.2 Fundamental interactions	14
³³	2.2.3 Gauge Bosons	19
³⁴	2.3 Electroweak unification and the Higgs mechanism	21
³⁵	2.3.1 Spontaneous symmetry breaking	29
³⁶	2.3.2 Higgs mechanism	33
³⁷	2.3.3 Masses of the gauge bosons	35

38	2.3.4	Masses of the fermions	36
39	2.3.5	The Higgs field	37
40	2.3.6	Higgs boson production mechanisms at LHC.	38
41	2.3.7	Higgs decay channels	42
42	2.4	Associated Production of Higgs Boson and Single Top Quark.	43
43	2.5	The CP-mixing phase	47
44	3	The CMS experiment at the LHC	48
45	3.1	Introduction	48
46	3.2	The LHC	49
47	3.3	The CMS experiment	53
48	4	Search for production of a Higgs boson and a single top quark in multilepton final states in pp collisions at $\sqrt{s} = 13$ TeV	55
50	4.1	Introduction	55
51	4.2	Data and MC Samples	57
52	4.2.1	Full 2016 dataset and MC samples	57
53	4.2.2	Triggers	60
54	4.2.2.1	Trigger efficiency scale factors	60
55	4.3	Object Identification and event selection	61
56	4.3.1	Jets and b tagging	61
57	4.3.2	Lepton selection	62
58	4.3.3	Lepton selection efficiency	63
59	4.4	Background predictions	64
60	4.5	Signal discrimination	65
61	4.5.1	Classifiers response	69
62	4.6	Additional discriminating variables	72

63	5 The CMS forward pixel detector	75
64	5.0.1 The phase 1 FPix upgrade	75
65	5.0.2 FPix module production line	75
66	5.0.3 The Gluing stage	75
67	5.0.4 The Encapsulation stage	75
68	5.0.5 The FPix module production yields	75
69	Bibliography	75
70	References	76

⁷¹ List of Figures

72	1.1	^{14}N neutron capture in a PECVD polymerized pyridine film. The Q-value of this reaction is 626 keV. Taken from [22]	1
74	2.1	Standard model of particle physics.	6
75	2.2	WI transformations between quarks	13
76	2.3	Fundamental interactions in nature.	14
77	2.4	SM interactions diagrams	15
78	2.5	Neutral current processes	22
79	2.6	Spontaneous symmetry breaking mechanism	29
80	2.7	SSB Potential form	30
81	2.8	Potential for complex scalar field	31
82	2.9	SSB mechanism for complex scalar field	32
83	2.10	Proton-Proton collision	39
84	2.11	Higgs production mechanism Feynman diagrams	40
85	2.12	Higgs production cross section and decay branching ratios	41
86	2.13	Associated Higgs production mechanism Feynman diagrams	43
87	2.14	Cross section for tHq process as a function of C_t	46
88	3.1	ref. C.Lefevre, “The CERN accelerator complex,” (2008). CERN-DI- 0812015.	50

90	3.2	ref. J.-L. Caron , “Layout of the LEP tunnel including future LHC in-	
91		frastructures.. L’ensemble du tunnel LEP avec les futures infrastructures	
92		LHC.”, https://cds.cern.ch/record/841542 (Nov, 1993). AC Collection.	
93		Legacy of AC. Pictures from 1992 to 2002..	51
94	3.3	ref. ACTeam, “Diagram of an LHC dipole magnet. Schéma d’un aimant	
95		dipôle du LHC,” (1999). CERN-DI-9906025.	52
96	3.4	ref: CMS Collaboration, “Detector Drawings”, CMS-PHO-GEN-2012-002,	
97		http://cds.cern.ch/record/1433717 , 2012.	54
98	4.1	The two leading-order diagrams of tHq production.	56
99	4.2	Input variables to the BDT for signal discrimination normalized.	66
100	4.3	Input variables to the BDT for signal discrimination not normalized. . .	68
101	4.4	BDT inputs as seen by TMVA against $t\bar{t}$	69
102	4.5	BDT inputs as seen by TMVA against $t\bar{t}V$	70
103	4.6	Correlation matrices for the input variables in the TMVA.	71
104	4.7	MVA classifiers performance.	71
105	4.8	Additional discriminating variables distributions.	73

¹⁰⁶ List of Tables

107	2.1	Fermions of the SM.	7
108	2.2	Leptons properties.	10
109	2.3	Quarks properties.	10
110	2.4	Fermion weak isospin and weak hypercharge multiplets.	12
111	2.5	Fundamental interactions features.	16
112	2.6	SM gauge bosons.	21
113	2.7	Higgs boson properties.	38
114	2.8	Predicted branching ratios for a SM Higgs boson with $m_H = 125 \text{ GeV}/c^2$	42
115	2.9	Predicted SM cross sections for tH production at $\sqrt{s} = 13 \text{ TeV}$	44
116	2.10	Predicted enhancement of the tHq cross sections at LHC	46
117	4.1	Signal samples and their cross section and branching fraction.	57
118	4.2	κ_V and κ_t combinations.	58
119	4.3	List of background samples used in this analysis (CMSSW 80X).	59
120	4.4	Leading-order $t\bar{t}W$ and $t\bar{t}Z$ samples used in the signal BDT training. . .	59
121	4.5	Table of high-level triggers that we consider in the analysis.	60
122	4.6	Trigger efficiency scale factors and associated uncertainties.	61
123	4.7	Requirements on each of the three muon selections.	62
124	4.8	Criteria for each of the three electron selections.	63

125	4.9 MVA input discriminating variables	67
126	4.10 TMVA input variables ranking for BDTA_GRAD method	72
127	4.11 TMVA configuration used in the BDT training.	72
128	4.12 ROC-integral for all the testing cases.	74

¹²⁹ Chapter 1

¹³⁰ INTRODUCTION

Figure 1.1: ^{14}N neutron capture in a PECVD polymerized pyridine film. The Q-value of this reaction is 626 keV. Taken from [22]

¹³¹ Chapter 2

¹³² Theoretical approach

¹³³ 2.1 Introduction

¹³⁴ The physical description of the universe is a challenge that physicists have faced by
¹³⁵ making theories that refine existing principles and proposing new ones in an attempt
¹³⁶ to embrace emerging facts and phenomena. By early 1800's, there were separate the-
¹³⁷ ories describing electric and magnetic phenomena, gravitational force and light. The
¹³⁸ invention of the electric battery by Alessandro Volta in 1800, the discovery of the
¹³⁹ magnetic effects of the electric current by Oersted and Ampere (1820), and the gen-
¹⁴⁰ eration of electric current using changing magnetic fields by Faraday (1831) represent
¹⁴¹ the first steps in the way to create a unified theory of electromagnetism [1].

¹⁴²

¹⁴³ The unification was carried out by James Clerk Maxwell who was able to merge elec-
¹⁴⁴ tricity and magnetism in a set of 20 equations known as "general equations of the
¹⁴⁵ electromagnetic field," relating the observables that describe the experimental laws of
¹⁴⁶ the electromagnetism. By combining these equations, Maxwell found a wave equation
¹⁴⁷ and propose the existence of the "electromagnetic waves." The predicted propagation

148 speed of the electromagnetic waves turned out to be the same as the speed of light,
149 therefore, the natural conclusion was that light is an electromagnetic wave [4]. By
150 1900, waves were considered a perturbation of a material medium which in the case
151 of the electromagnetic waves was identified as the “*Luminiferous Ether*”.

152

153 By 1900, Max Planck came out with the idea that radiation is quantized [5] and Albert
154 Einstein in 1905 made use of that hypothesis to propose the existence of the light
155 quantum, the “*photon*”, in order to explain the photoelectric effect [6]. The well-
156 known quantum revolution in physics started and the idea of particle-wave duality
157 of photons as a natural behavior was developed and later extended to electrons and
158 to all kind of particles in nature. The development of a quantum theory allowed to
159 predict a set of non-common sense effects like the quantum tunneling and quantum
160 entanglement, however, quantum theory was separated from the recently unified elec-
161 tromagnetism.

162

163 In 1905, Einstein also published two more papers; one aimed to describe his statistical
164 molecular theory of liquids and how it can be used to describe Brownian motion [7].
165 At that time the existence of the atoms and molecules were not fully demonstrated
166 but Einstein’s theory provided an explanation as well as predictions based on the
167 their existence. Jean Perrin in 1908 conducted experiments that confirmed Einstein’s
168 predictions. The other paper described the relationship between space and time [8],
169 unifying the notion of space and time into one entity known as “*spacetime*” that treats
170 space and time at the same level and then discards the absoluteness of time. The
171 new theory known as special relativity, supersedes the Galilean relativity principle
172 and postulates exceptional effects like the time dilation, length contraction and mass-

173 energy equivalence through the most famous formula in physics [9]

$$E = mc^2. \quad (2.1)$$

174 Generalization of the special relativity was presented in 1916 and includes a gener-
175 alization of Newton's law of universal gravitation, becoming a unified description of
176 gravity as a geometric property of space and time. Einstein's predictions include the
177 existence of black holes and the recently observed "*gravitational waves*" [10].

178 At the end of 1940s Julian Schwinger [11] and Richard P. Feynman [12], based in
179 the work of Sin-Itiro Tomonaga [13], developed an electromagnetic theory consistent
180 with special relativity and quantum mechanics that describes how matter and light
181 interact; so-called "quantum eletrodynamics" (QED) had born.

182

183 QED has become the guide in the development of theories that describe the universe.
184 It was the first example of a quantum field theory (QFT), which is the theoretical
185 framework for building quantum mechanical models that describes particles and their
186 interactions. QFT is composed of a set of mathematical tools that combines classical
187 fields, special relativity, and quantum mechanics while keeping the quantum point
188 particles and locality ideas. This chapter gives an overview of the SM, starting with
189 the SM particle content, followed by a description of the electroweak interaction, the
190 Higgs boson and the associated production of Higgs boson and a single top quark
191 (tH). The description contained in this chapter is based on references [1–3].

192 2.2 Standard model of particle physics

193 Particle physics at the fundamental level is modeled in terms of a collection of in-
194 teracting particles and fields in a theory known as the “standard model of particle
195 physics (SM)”¹.

196 The full picture of the SM is composed of three fields², whose excitations are inter-
197 preted as particles called mediators or force-carriers; a set of fields, whose excitations
198 are interpreted as elementary particles, interacting through the exchange of those
199 mediators and a field that give the mass to elementary particles. Figure 2.1 shows an
200 scheme of the SM particles organization. In addition to the particles in the scheme,
201 their corresponding anti-particles, with opposite quantum numbers, are also part of
202 the picture; some particles are their own anti-particles, like photon or Higgs, or anti-
203 particle is already listed like in the W^+ and W^- case.

204

205 The mathematical formulation of the SM is based on group theory and the use of
206 Noether’s theorem [17] which states that for a physical system modeled by a La-
207 grangian that is invariant under a group of transformations a conservation law is
208 expected. For instance, a system described by a time-independent Lagrangian is
209 invariant (symmetric) under time changes (transformations) with the total energy
210 conservation law as the expected conservation law. In QED, the Q operator is the
211 generator of the $U(1)$ symmetry which according to the Noether’s theorem means
212 that there is a conserved charge; this conserved charge is the electric charge and thus
213 the law conservation of electric charge is established.

¹ The formal and complete treatment of the SM is out of the scope of this document, however a plenty of textbooks describing it at several levels are available in the literature. The treatment in “An Introduction To Quantum Field Theory (Frontiers in Physics)” by Michael E. Peskin and Dan V. Schroeder is quite comprehensive and detailed.

² Note that gravitational field is not included in the standard model formulation

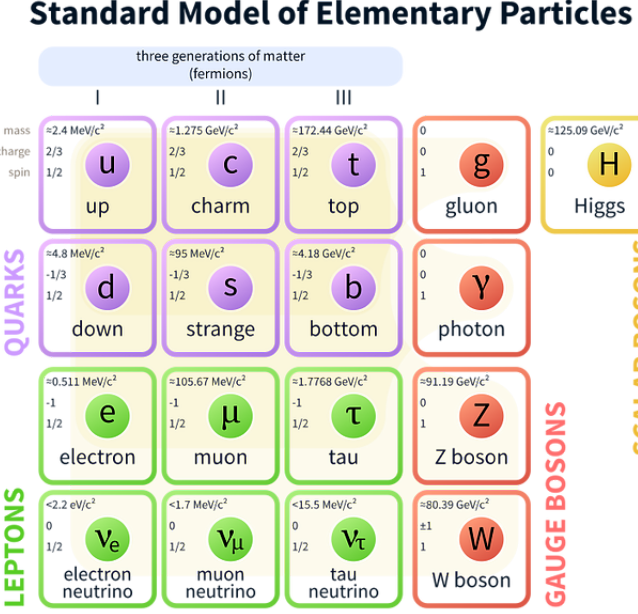


Figure 2.1: Schematic representation of the Standard model of particle physics. SM is a theoretical model intended to describe three of the four fundamental forces of the universe in terms of a set of particles and their interactions. [18].

214

215 In the SM, the symmetry group $SU(3)_C \otimes SU(2)_L \otimes U(1)_Y$ describes three of the
 216 four fundamental interactions in nature(see section 2.2.2): strong interaction(SI),
 217 weak interaction(WI) and electromagnetic interactions (EI) in terms of symmetries
 218 associated to physical quantities:

- 219 • Strong: $SU(3)_C$ associated to color charge
 220 • Weak: $SU(2)_L$ associated to weak isospin and chirality
 221 • Electromagnetic: $U(1)_Y$ associated to weak hypercharge and electric charge

222 It will be shown that the electromagnetic and weak interactions are combined in
 223 the so-called electroweak interaction where chirality, hypercharge, weak isospin and
 224 electric charge are the central concepts.

225 2.2.1 Fermions

226 The basic constituents of the ordinary matter at the lowest level, which form the set
 227 of elementary particles in the SM formulation, are quarks and leptons. All of them
 228 have spin 1/2, therefore they are classified as fermions since they obey Fermi-Dirac
 229 statistics. In both cases, they come in six “flavors” and are organized in three gener-
 230 ations, or families, as shown in table 2.1.

231

232 There is a mass hierarchy between generations where the higher generation particles
 233 decays to the lower one which can explain why the ordinary matter is made of particles
 234 in the first generation. In the SM, neutrinos are modeled as massless particles so they
 235 are not subject to this mass hierarchy; however, today it is known that neutrinos are
 236 massive so the hierarchy could be restated. The reason behind this mass hierarchy is
 237 one of the most important open questions in particle physics, and it becomes more
 238 puzzling when noticing that the mass difference between first and second generation
 239 fermions is small compared to the mass difference with respect to the third generation.
 240 Usually, the second and third generation fermions are produced in high energy pro-
 241 cesses, like the ones recreated in the particle accelerators.

Generation				
	Type	1st	2nd	3rd
Leptons	Charged	Electron (e)	Moun(μ)	Tau (τ)
	Neutral	Electron neutrino (ν_e)	Muon neutrino (ν_μ)	Tau neutrino (ν_τ)
Quarks	Up-type	Up (u)	Charm (c)	Top (t)
	Down-type	Down (d)	Starnge (s)	Bottom (b)

Table 2.1: Fermions of the SM. Quarks and leptons comes in six flavors each and are organized in three generations or families composed of two pairs of closely related particles. The close relationship is motivated by the fact that WI between leptons is limited to the members of the same generation. Generations differs by mass in a way that have been interpreted as a masss hierarchy.

242

243 **2.2.1.1 Leptons**

244 A lepton is an elementary particle that is not subject to the SI. As seen in table 2.1,
 245 there are two types of leptons, the charged ones (electron, muon and tau) and the
 246 neutral ones (the three neutrinos). The electric charge (Q) is the property that gives
 247 leptons the ability to participate in the EI. From the classical point of view, Q plays
 248 a central role determining, among others, the strength of the electric field through
 249 which the electromagnetic force is exerted. It is clear that neutrinos are not affected
 250 by EI because they don't carry electric charge.

251

252 Another feature of the leptons that is fundamental in the mathematical description
 253 of the SM is the chirality, which is closely related to spin and helicity. Helicity de-
 254 fine the handedness of a particle by relating its spin and momentum such that if
 255 they are parallel then the particle is right-handed; if spin and momentum are an-
 256 tiparallel the particle is said to be left-handed. The study of parity conservation
 257 (or violation) in β -decay have shown that only left-handed electrons/neutrinos or
 258 right-handed positrons/anti-neutrinos are created [19]; the inclusion of that feature
 259 in the theory was reached by using projection operators for helicity, however, helicity
 260 is frame dependent for massive particles which makes it not Lorentz invariant and
 261 then another related attribute has to be used: *chirality*.

262

263 Chirality is a purely quantum attribute which makes it not so easy to describe in
 264 graphical terms but it defines how the wave function of a particle transforms under
 265 certain rotations. As with helicity, there are two chiral states, left-handed chiral
 266 (L) and right-handed chiral (R). In the highly relativistic limit where $E \approx p \gg m$
 267 helicity and chirality converge, becoming exactly the same for massless particles. In

268 the following when referring to left-handed (right-handed) it means left-handed chiral
 269 (right-handed chiral). The fundamental fact about chirality is that while EI and SI
 270 are not sensitive to chirality, in WI left-handed and right-handed fermions are treated
 271 asymmetrically, such that only left handed fermions and right-handed anti-fermions
 272 are allowed to couple to WI mediators, which is a violation of parity. The way to
 273 translate this statement in a formal mathematical formulation is based on the isospin
 274 symmetry group $SU(2)_L$.

275 Each generation of leptons is seen as a weak isospin doublet.³ The left-handed charged
 276 lepton and its associated left-handed neutrino are arranged in doublets of weak isospin
 277 $T=1/2$ while their right-handed partners are singlets:

$$\begin{pmatrix} \nu_l \\ l \end{pmatrix}_L, l_R := \begin{pmatrix} \nu_e \\ e \end{pmatrix}_L, \begin{pmatrix} \nu_\mu \\ \mu \end{pmatrix}_L, \begin{pmatrix} \nu_\tau \\ \tau \end{pmatrix}_L, e_R, \mu_R, \tau_R, \nu_{eR}, \nu_{\mu R}, \nu_{\tau R} \quad (2.2)$$

278 The isospin third component refers to the eigenvalues of the weak isospin operator
 279 which for doublets is $T_3 = \pm 1/2$, while for singlets it is $T_3 = 0$. The physical meaning
 280 of this doublet-singlet arrangement falls in that the WI couples the two particles in
 281 the doublet by exchanging the interaction mediator while the singlet member is not
 282 involved in WI. The main properties of the leptons are summarized in table 2.2.

283

284 Altough all three flavor neutrinos have been observed, their masses remain unknown
 285 and only some estimations have been made [20]. The main reason is that the fla-
 286 vor eigenstates are not the same as the mass eigenstates which imply that when a
 287 neutrino is created its mass state is a linear combination of the three mass eigen-
 288 states and experiments can only probe the squared difference of the masses. The
 289 Pontecorvo-Maki-Nakagawa-Sakata (PMNS) mixing matrix encode the relationship

³ The weak isospin is an analogy of the isospin symmetry in strong interaction where neutron and proton are affected equally by strong force but differ in their charge.

290 between flavor and mass eigenstates.

Lepton	Q(e)	T_3	L_e	L_μ	L_τ	Mass (MeV/c ²)	Lifetime (s)
Electron (e)	-1	-1/2	1	0	0	0.5109989461(31)	Stable
Electron neutrino(ν_e)	0	1/2	1	0	0	Unknown	Unknown
Muon (μ)	-1	-1/2	0	1	0	105.6583745(24)	$2.1969811(22) \times 10^{-6}$
Muon neutrino (ν_μ)	0	1/2	0	1	0	Unknown	Unknown
Tau (τ)	-1	-1/2	0	0	1	1776.86(12)	$290.3(5) \times 10^{-15}$
Tau neutrino (τ_μ)	0	1/2	0	0	1	Unknown	Unknown

Table 2.2: Leptons properties [21]. Q: electric charge, T_3 : weak isospin. Only left-handed leptons and right-handed anti-leptons participate in the WI. Anti-particles with inverted T_3 , Q and lepton number complete the leptons set but are not listed. Right-handed leptons and left-handed anti-leptons, neither listed, form weak isospin singlets with $T_3 = 0$ and do not take part in the weak interaction.

291

292 2.2.1.2 Quarks

293 Quarks are the basic constituents of protons, neutrons and other non-elementary
 294 particles. The way quarks join to form bound states, called “hadrons”, is through the
 295 SI. Quarks are affected by all the fundamental interactions which means that they
 296 carry all the four types of charges: color, electric charge, weak isospin and mass.

Flavor	Q(e)	I_3	T_3	B	C	S	T	B'	Y	Color	Mass (MeV/c ²)
Up (u)	2/3	1/2	1/2	1/3	0	0	0	0	1/3	r,b,g	$2.2^{+0.6}_{-0.4}$
Charm (c)	2/3	0	1/2	1/3	1	0	0	0	4/3	r,b,g	$1.28 \pm 0.03 \times 10^3$
Top(t)	2/3	0	1/2	1/3	0	0	1	0	4/3	r,b,g	$173.1 \pm 0.6 \times 10^3$
Down(d)	-1/3	-1/2	-1/2	1/3	0	0	0	0	1/3	r,b,g	$4.7^{+0.5}_{-0.4}$
Strange(s)	-1/3	0	-1/2	1/3	0	-1	0	0	-2/3	r,b,g	96^{+8}_{-4}
Bottom(b)	-1/3	0	-1/2	1/3	0	0	0	-1	-2/3	r,b,g	$4.18^{+0.04}_{-0.03} \times 10^3$

Table 2.3: Quarks properties [21]. Q: electric charge, I_3 : isospin, T_3 : weak isospin, B: baryon number, C: charmness, S: strangeness, T: topness, B' : bottomness, Y: hypercharge. Anti-quarks posses the same mass and spin as quarks but all charges (color, flavor numbers) have opposite sign.

297

298 Table 2.3 summarizes the features of quarks, among which the most particular is
 299 their fractional electric charge. Note that fractional charge is not a problem, given
 300 that quarks are not found isolated, but serves to explain how composed particles are
 301 formed out of two or more valence quarks⁴.

302

303 Color charge is the responsible for the SI between quarks and is the symmetry
 304 ($SU(3)_C$) that defines the formalism to describe SI. There are three colors: red (r),
 305 blue(b) and green(g) and their corresponding three anti-colors; thus each quark carries
 306 one color unit while anti-quarks carries one anti-color unit. As said above, quarks are
 307 not allowed to be isolated due to the color confinement effect, therefore their features
 308 have been studied indirectly by observing their bound states created when:

309 • one quark with a color charge is attracted by an anti-quark with the correspond-
 310 ing anti-color charge forming a colorless particle called a “meson.”

311 • three quarks (anti-quarks) with different color (anti-color) charges are attracted
 312 among them forming a colorless particle called a “baryon(anti-baryon).”

313 In the first version of the quark model (1964), M. Gell-Mann [22] and G. Zweig [23,24]
 314 developed a consistent way to classify hadrons according to their properties. Only
 315 three quarks (u, d, s) were involved in a scheme in which all baryons have baryon
 316 number $B=1$ and therefore quarks have $B=1/3$; non-baryons have $B=0$. The scheme
 317 organize baryons in a two-dimensional space ($I_3 - Y$); Y (hypercharge) and I_3 (isospin)
 318 are quantum numbers related by the Gell-Mann-Nishijima formula [25, 26]:

$$Q = I_3 + \frac{Y}{2} \quad (2.3)$$

⁴ Hadrons can contain an indefinite number of virtual quarks and gluons, known as the quark and gluon sea, but only the valence quarks determine hadrons' quantum numbers.

319 where $Y = B + S + C + T + B'$ are the quantum numbers listed in table 2.3. Baryon
 320 number is conserved in SI and EI which means that single quarks cannot be created
 321 but in pairs $q - \bar{q}$.

322

323 Similar to leptons, there are six quark flavors organized in three generations (see table
 324 2.1) and follow a mass hierarchy which again implies that higher generations decay
 325 to first generation quarks.

	Quarks			T_3	Y_W	Leptons			T_3	Y_W
Doublets	$(\frac{u}{d'})_L$	$(\frac{c}{s'})_L$	$(\frac{t}{b'})_L$	$(\frac{1/2}{-1/2})$	1/3	$(\nu_e)_L$	$(\nu_\mu)_L$	$(\nu_\tau)_L$	$(\frac{1/2}{-1/2})$	-1
Singlets	u_R	c_R	t_R	0	4/3	ν_{eR}	$\nu_{\mu R}$	$\nu_{\tau R}$	0	-2
	d'_R	s'_R	b'_R	0	-2/3	e_R	μ_R	τ_R		

Table 2.4: Fermion weak isospin and weak hypercharge multiplets. Weak hypercharge is calculated through the Gell-Mann-Nishijima formula 2.3 but using the weak isospin and charge for quarks.

326

327 Isospin doublets of quarks are also defined (see table 2.4) and as for neutrinos, the
 328 mass eigenstates are not the same as the WI eigenstates which means that members of
 329 different quark generations are connected by the WI mediator; thus, up-type quarks
 330 are coupled not to down-type quarks directly but to a superposition of down-type
 331 quarks (q'_d) via WI according to:

$$q'_d = V_{CKM} q_d$$

332

$$\begin{pmatrix} d' \\ s' \\ b' \end{pmatrix} = \begin{pmatrix} V_{ud} & V_{us} & V_{ub} \\ V_{cd} & V_{cs} & V_{cb} \\ V_{td} & V_{ts} & V_{tb} \end{pmatrix} \begin{pmatrix} d \\ s \\ b \end{pmatrix} \quad (2.4)$$

333 where V_{CKM} is known as Cabibbo-Kobayashi-Maskawa (CKM) mixing matrix [27,28].

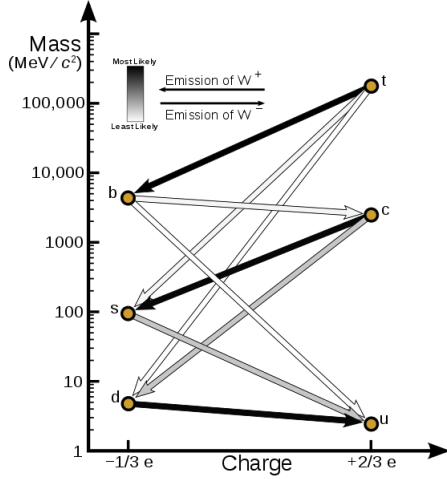


Figure 2.2: Transformations between quarks through WI. Higher generations quarks decay to first generation quarks by emitting a W boson. The arrow color indicates the likelihood of the transition according to the grey scale in the top left side which represent the CKM matrix parameters [29].

334 The weak decays of quarks are represented in the diagram of figure 2.2; again the
 335 CKM matrix plays a central role since it contains the probabilities for the different
 336 quark decay channels, in particular, note that quark decays are greatly favored be-
 337 tween generation members.

338

339 CKM matrix is a 3×3 unitary matrix parametrized by three mixing angles and the
 340 *CP-mixing phase*; the latter is the parameter responsible for the CP-violation in the
 341 SM. The fact that the b quark decays almost all the times to a top quark is exploited
 342 in this thesis when making the selection of the signal events by requiring the presence
 343 of a jet tagged as a jet coming from a b quark in the final state. The effect of the
 344 *CP-mixing phase* on the cross section of associated production of Higgs boson and a
 345 single top process is also explored in this thesis.

Fundamental interactions.

Illustration: Typoform

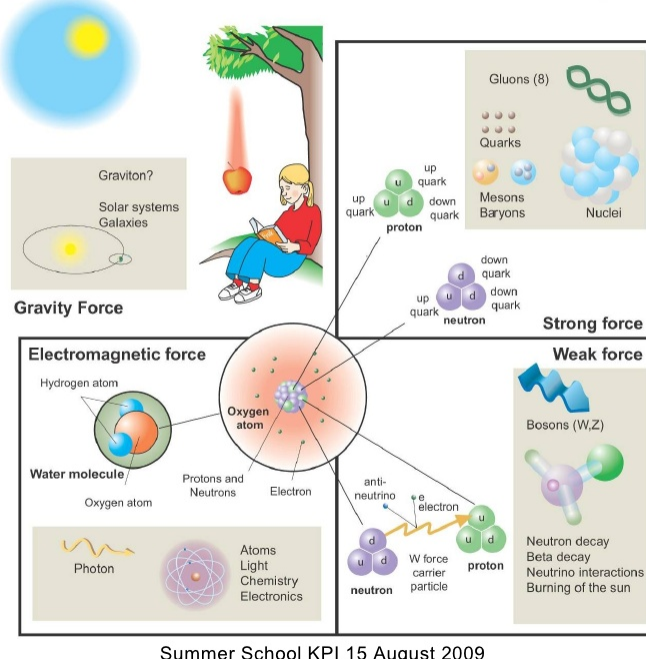


Figure 2.3: Fundamental interactions in nature. Despite the many manifestations of forces in nature, we can track all of them back to one of the fundamental interactions. The most common forces are gravity and electromagnetic given that all of us are subject and experience them in everyday life.

346 2.2.2 Fundamental interactions

347 Even though there are many manifestations of force in nature, like the ones represented in figure 2.3, we can classify all of them into one of four fundamental interactions:

- 350 • *Electromagnetic interaction (EI)* affect particles that are “electrically charged,”
 351 like electrons and protons. It is described by QED combining quantum mechanics,
 352 special relativity and electromagnetism in order to explain how particles
 353 with electric charge interact through the exchange of photons, therefore, one
 354 says that “Electromagnetic Force” is mediated by “photons”. Figure 2.4a) shows
 355 a graphical representation, known as “feynman diagram”, of electron-electron

356 scattering.

357 • *Strong interaction (SI)* described by Quantum Chromodynamics (QCD). Hadrons
 358 like proton and neutron have internal structure given that they are composed
 359 of two or more valence quarks⁵. Quarks have fractional electric charge which
 360 means that they are subject to electromagnetic interaction and in the case of the
 361 proton they should break apart due to electrostatic repulsion; however, quarks
 362 are held together inside the hadrons against their electrostatic repulsion by the
 363 “Strong Force” through the exchange of “gluons.” The analog to the electric
 364 charge is the “color charge”. Electrons and photons are elementary particles
 365 as quarks but they don’t carry color charge, therefore they are not subject to
 366 SI. The feynman diagram for gluon exchange between quarks is shown in figure
 367 2.4b).

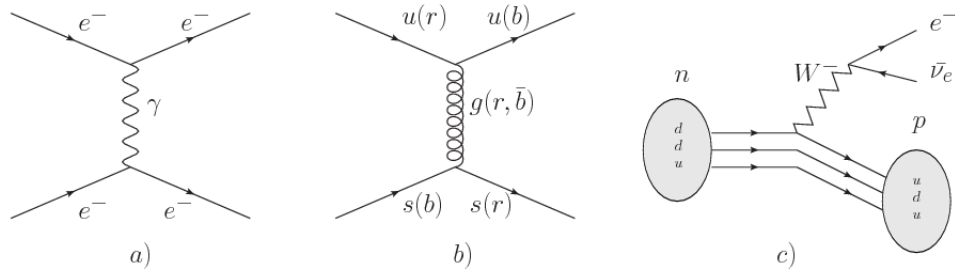


Figure 2.4: Feynman diagrams representing the interactions in SM; a) EI: e - e scattering; b) SI: gluon exchange between quarks ; c) WI: β -decay

368 • *Weak interaction (WI)* described by the Weak theory (WT), is responsible for
 369 instance for the radioactive decay in atoms and proton-proton (pp) fusion within
 370 the sun. Quarks and leptons are the particles affected by the weak interaction
 371 and posses a property called “flavor charge” which can be changed by emitting
 372 or absorbing one weak force mediator; they comes in six flavors each (see 2.2.1).
 373 There are three mediators of the “Weak force” known as “Z” boson in the case of

⁵ particles made of four and five quarks are exotic states not so common

374 electrically neutral changes and “ W^\pm ” bosons in the case of electrically charged
 375 changes. The “weak isospin” is the WI analog to electric charge in EI and color
 376 charge in SI and define how quarks and leptons are affected by the weak force.
 377 Figure 2.4c) shows the feynman diagram of β -decay where a newtron (n) is
 378 transformed in a proton (p) by emmiting a W^- particle. Since this thesis is in
 379 the frame of the electroweak interaction, a more detailed description of it will
 380 be given in section 2.3

381 • *Gravitational interaction (GI)* described by General Theory of Relativity (GR).
 382 It is responsible for the structure of galaxies and black holes as well as the
 383 expansion of the universe. As a classical theory, in the sense that it can be
 384 formulated without even appeal to the concept of quantization, it implies that
 385 the spacetime is a continuum and predictions can be made without limitation
 386 to the precision of the measurement tools which represent a direct contradiction
 387 of the quantum mechanics principles. Gravity is deterministic while quantum
 388 mechanics is probabilistic; despite that, efforts to develop a quantum theory of
 389 gravity have predicted the “graviton” as mediator of the Gravitational force⁶.

Interaction	Acts on	Relative strength	Range (m)	Mediators
Electromagnetic (QED)	Electrically charged particles	10^{-2}	Infinite	Photon
Strong (QCD)	Quarks and gluons	1	10^{-15}	Gluon
Weak (WI)	Leptons and quarks	10^{-6}	10^{-18}	W^\pm , Z
Gravitational (GI)	Massive particles	10^{-39}	Infinite	Graviton

Table 2.5: Fundamental interactions features [30].

390

391 Table 2.5 summarizes the main features of the fundamental interactions. The rela-
 392 tive strength of the fundamental forces reveals the meaning of strong and weak;

⁶ Actually a wide variety of theories have been developed in an attempt to describe gravity; some famous examples are string theory and supergravity.

393 a context where the relative strength of the SI is 1, the EI is about hundred times
 394 weaker and WI is about million times weaker than the SI. A good description on
 395 how the relative strength and range of the fundamental interactions are calculated
 396 can be found in references [30, 31]. In the everyday life, only EI and GI are explicitly
 397 experienced due to the range of these interactions; i.e., at the human scale distances
 398 only EI and GI have appreciable effects, in contrast to SI which at distances greater
 399 than 10^{-15} m become negligible.

400

401 QED was built successfully on the basis of the classical electrodynamics theory of
 402 Maxwell and Lorentz (CED), following theoretical and experimental requirements
 403 imposed by

- 404 • lorentz invariance: independence on the reference frame.
- 405 • locallity: interacting fields are evaluated at the same space-time point to avoid
 406 action at a distance.
- 407 • renormalizability: physical predictions are finite and well defined
- 408 • particle spectrum, symmetries and conservation laws already known must emerge
 409 from the theory.
- 410 • gauge invariance.

411 The gauge invariance requirement reflects the fact that the fundamental fields cannot
 412 be directly measured but associated fields which are the observables. Electric (“**E**”)
 413 and magnetic (“**B**”) fields in CED are associated with the electric scalar potential
 414 “**V**” and the vector potential “**A**”. In particular, **E** can be obtained by measuring
 415 the change in the space of the scalar potential (ΔV); however, two scalar potentials

416 differing by a constant “f” correspond to the same electric field. The same happens
 417 in the case of the vector potential “ \mathbf{A} ”; thus, different configurations of the associated
 418 fields result in the same set of values of the observables. The freedom in choosing
 419 one particular configuration is known as “gauge freedom”; the transformation law
 420 connecting two configurations is known as “gauge transformation” and the fact that
 421 the observables are not affected by a gauge transformation is called “gauge invariance”.
 422 When the gauge transformation:

$$\begin{aligned}\mathbf{A} &\rightarrow \mathbf{A} - \nabla f \\ V &\rightarrow V - \frac{\partial f}{\partial t}\end{aligned}\tag{2.5}$$

423 is applied to Maxwell equations, they are still satisfied and the fields remain invariant.
 424 Thus, the classical electrodynamics theory is invariant under gauge transformations
 425 and is called a “gauge theory”. The set of all gauge transformations form the “sym-
 426 metry group” of the theory, which according to the group theory, has a set of “group
 427 generators”. The number of group generators determine the number of “gauge fields”
 428 of the theory.

429

430 As mentioned in the first lines of section 2.2, QED has one symmetry group ($U(1)$)
 431 with one group generator (the Q operator) and one gauge field (the electromagnetic
 432 field A^μ). In CED there is not a clear definition, beyond the historical convention, of
 433 which fields are the fundamental and which are the associated, but in QED it is clear
 434 that the fundamental field is A^μ . When a gauge theory is quantized, the gauge field
 435 is quantized and its quanta is called “gauge boson”. The word boson characterize
 436 particles with integer spin which obey Bose-Einstein statistics.

437

438 As will be detailed in section 2.3, interactions between particles in a system can be
 439 obtained by considering first the Lagrangian density of free particles in the system,
 440 which of course is incomplete because the interaction terms have been left out, and
 441 demanding global phase transformation invariance. Global phase transformation in-
 442 variance means that a gauge transformation is performed identically to every point
 443 in the space⁷ and the Lagrangian remains invariant. Then, the global transformation
 444 is promoted to a local phase transformation (this time the gauge transformation de-
 445 pends on the position in space) and again invariance is required.

446

447 Due to the space dependence of the local transformation, the Lagrangian density is
 448 not invariant anymore. In order to restate the gauge invariance, the gauge covariant
 449 derivative is introduced in the Lagrangian and with it the gauge field responsible for
 450 the interaction between particles in the system. The new Lagrangian density is gauge
 451 invariant, includes the interaction terms needed to account for the interactions and
 452 provide a way to explain the interaction between particles through the exchange of
 453 the gauge boson.

454 This recipe was used to build QED and the theories that aim to explain the funda-
 455 mental interactions.

456 2.2.3 Gauge Bosons

457 The importance of the gauge bosons comes from the fact that they are the force
 458 mediators or force carriers. The features of the gauge bosons reflect the features of
 459 the fields they represent; these features are extracted from the Lagrangian density used
 460 to describe the interactions. In section 2.3, it will be shown how the gauge bosons

⁷ Here space corresponds to the 4-dimensional space i.e. space-time.

461 of the EI and WI emerge from the electroweak Lagrangian. The SI gauge bosons
 462 features are also extracted from the SI Lagrangian but it is not detailed in this
 463 document. Here, the main features of the SM gauge bosons will be briefly presented
 464 and summarized in table 2.6.

465 • **Photon.** EI occurs when the photon couples to (is exchanged between) particles
 466 carrying electric charge; however, the photon itself does not carry electric charge,
 467 therefore, there is no coupling between photons. Given that the photon is
 468 massless the EI is of infinite range i.e. electrically charged particles interact
 469 even if they are located far away one from each other; that also means that
 470 photons always move with the speed of light.

471 • **Gluon.** SI is mediated by gluons, which same as photons are massless. They
 472 carry one unit of color charge and one unit of anticolor charge which means that
 473 gluons couples to other gluons. As a result, the range of the SI is not infinite
 474 but very short due to the attraction between gluons, giving rise to the “color
 475 confinement” which explains why color charged particles cannot be isolated but
 476 live within composited particles, like quarks inside protons.

477 • **W, Z.** The EWI mediators, W^\pm and Z, are massive which explain its short-
 478 range. Given that the WI is the only interaction that can change the flavor
 479 of the interacting particles, the W boson is the responsible for the nuclear
 480 transmutation where a neutron is converted in a proton or vice versa with the
 481 involvement of an electron and a neutrino. The Z boson is the responsible of the
 482 neutral weak processes like neutrino elastic scattering where no electric charge
 483 but momentum transference is involved. WI gauge bosons carry isospin charge
 484 which makes possible the interaction between them.

Interaction	Mediator	Electric charge (e)	Color charge	Weak Isospin	mass (GeV/c ²)
Electromagnetic	Photon (γ)	0	No	0	0
Strong	Gluon (g)	0	Yes -octet	No	0
Weak	W^\pm Z	± 1 0	No No	± 1 0	80.385 ± 0.015 91.188 ± 0.002

Table 2.6: SM gauge bosons main features [21].

485

486 **2.3 Electroweak unification and the Higgs**

487 **mechanism**

488 Physicist dreams of building a theory that contains all the interactions in one single
 489 interaction, i.e. showing that at some scale in energy all the four fundamental in-
 490 teractions are unified and only one interaction emerges in a “Theory of everything”.
 491 The first sign of the feasibility of such unification comes from success in the con-
 492 struction of the CED. Einstein spent years trying to reach that dream, which by
 493 1920 only involved electromagnetism and gravity, with no success; however, a new
 494 partial unification was achieved in the 1960’s, when S.Glashow [14], A.Salam [15] and
 495 S.Weinberg [16] independently proposed that electromagnetic and weak interactions
 496 are two manifestations of a more general interaction called “electroweak interaction.”
 497 QCD and EWT were developed in parallel and following the useful prescription pro-
 498 vided by QED and the gauge invariance principles.

499

500 The theory of weak interactions was capable of explaining the β -decay and in general
 501 the processes mediated by W^\pm bosons. However, there were some processes like the
 502 “ $\nu_\mu - e$ scattering” which would require the exchange of two W bosons (see figure 2.5
 503 top diagrams) giving rise to divergent loop integrals and then non finite predictions.

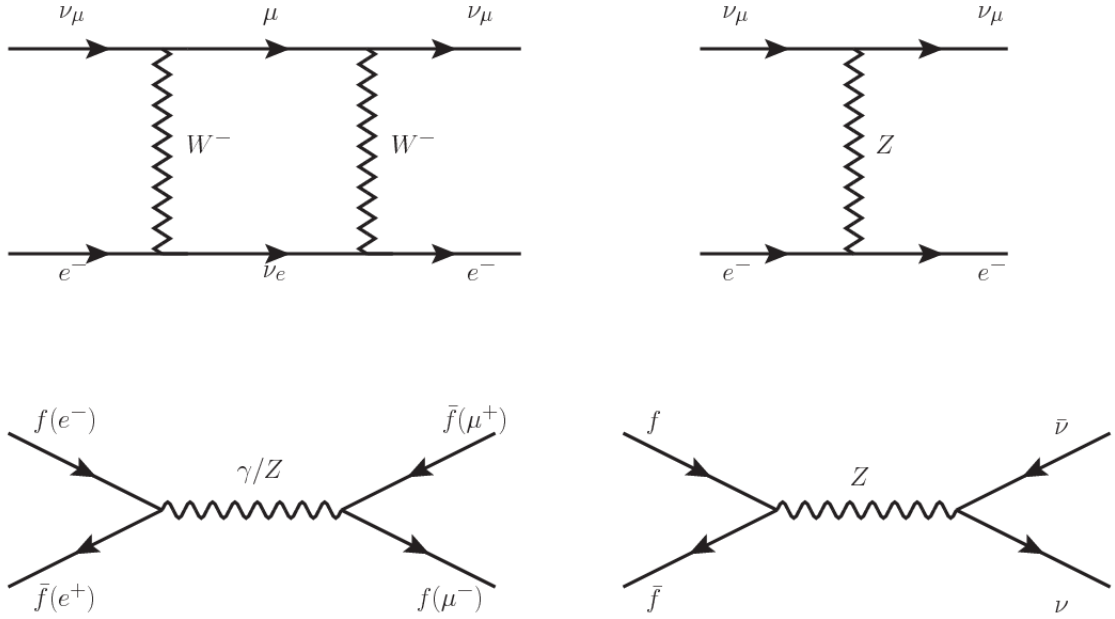


Figure 2.5: Top: $\nu_\mu - e^-$ scattering going through charged currents (left) and neutral currents (right). Bottom: neutral current processes for charged fermions (left) and involving neutrinos (right). While neutral current processes involving only charged fermions can proceed through EI or WI, those involving neutrinos can only proceed via WI.

504 By including neutral currents involving fermions via the exchange of neutral bosons
 505 Z , those divergences are compensated and the predictions become realistic.
 506 Neutral weak interaction vertices conserve flavor in the same way as the electromag-
 507 netic vertices do, but additionally, the Z boson can couple to neutrinos which implies
 508 that processes involving charged fermions can proceed through EI or WI but processes
 509 involving neutrinos can proceed only through WI.

510

511 The prescription to build a gauge theory of the WI consist of proposing a free field La-
 512 grangian density that includes the particles involved; next, by requesting invariance
 513 under global phase transformations first and generalizing to local phase transfor-
 514 mations invariance later, the conserved currents are identified and interactions are
 515 generated by introducing gauge fields. Given that the goal is to include the EI and

516 WI in a single theory, the group symmetry considered should be a combination of
 517 $SU(2)_L$ and $U(1)_{em}$, however the latter cannot be used directly because the EI treat
 518 left and right-handed particles indistinctly in contrast to the former. Fortunately, the
 519 weak hypercharge, which is a combination of the weak isospin and the electric charge
 520 (eqn 2.3) is suitable to be used since it is conserved by the EI and WI. Thus, the
 521 symmetry group to be considered is

$$G \equiv SU(2)_L \otimes U(1)_Y \quad (2.6)$$

522 The following treatment applies to any of the fermion generations but for simplicity
 523 the first generation of leptons will be considered [2, 3, 32, 33]. Also, the unified weak
 524 and electromagnetic interaction will be referred as “Electroweak Interaction (EWI).”
 525 Given the first generation of leptons

$$\psi_1 = \begin{pmatrix} \nu_e \\ e^- \end{pmatrix}_L, \quad \psi_2 = \nu_{eR}, \quad \psi_3 = e_R^- \quad (2.7)$$

526 the charged fermionic currents are given by

$$J_\mu \equiv J_\mu^+ = \bar{\nu}_{eL} \gamma_\mu e_L, \quad J_\mu^\dagger \equiv J_\mu^- = \bar{e}_L \gamma_\mu \nu_{eL} \quad (2.8)$$

527 and the free Lagrangian is given by

$$\mathcal{L}_0 = \sum_{j=1}^3 i\bar{\psi}_j(x) \gamma^\mu \partial_\mu \psi_j(x). \quad (2.9)$$

528 Mass terms are included directly in the QED and QCD free Lagrangians since they
 529 preserve the invariance under the symmetry transformations involved which treat
 530 left-handed and right-handed similarly, however mass terms of the form

$$m_W^2 W_\mu^\dagger(x) W^\mu(x) + \frac{1}{2} m_Z^2 Z_\mu(x) Z^\mu(x) - m_e \bar{\psi}_e(x) \psi_e(x) \quad (2.10)$$

531 which represent the mass of W^\pm , Z and electrons, are not invariant under G trans-
 532 formations, therefore the gauge fields described by the EWI are in principle massless.

533

534 Experiments have shown that the gauge fields are not massless; however, they have
 535 to acquire mass through a mechanism compatible with the gauge invariance; that
 536 mechanism is known as the “Higgs mechanism” and will be considered later in this
 537 section. The global transformations in the combined symmetry group G can be
 538 written as

$$\begin{aligned} \psi_1(x) &\xrightarrow{G} \psi'_1(x) \equiv U_Y U_L \psi_1(x), \\ \psi_2(x) &\xrightarrow{G} \psi'_2(x) \equiv U_Y \psi_2(x), \\ \psi_3(x) &\xrightarrow{G} \psi'_3(x) \equiv U_Y \psi_3(x) \end{aligned} \quad (2.11)$$

539 where U_L represent the $SU(2)_L$ transformation acting on the weak isospin doublet
 540 only and U_Y represent the $U(1)_Y$ transformation acting on all the weak isospin mul-
 541 tiplets. Explicitly

$$U_L \equiv \exp\left(i \frac{\sigma_i}{2} \alpha^i\right), \quad U_Y \equiv \exp(i y_i \beta) \quad (i = 1, 2, 3) \quad (2.12)$$

542 with σ_i the Pauli matrices and y_i the weak hypercharges. In order to promote the
 543 transformations from global to local while keeping the invariance, it is required that
 544 $\alpha^i = \alpha^i(x)$, $\beta = \beta(x)$ and the replacement of the ordinary derivatives by the covariant
 545 derivatives

$$\begin{aligned}
D_\mu \psi_1(x) &\equiv \left[\partial_\mu + ig\sigma_i W_\mu^i(x)/2 + ig'y_1 B_\mu(x) \right] \psi_1(x) \\
D_\mu \psi_2(x) &\equiv \left[\partial_\mu + ig'y_2 B_\mu(x) \right] \psi_2(x) \\
D_\mu \psi_3(x) &\equiv \left[\partial_\mu + ig'y_3 B_\mu(x) \right] \psi_3(x)
\end{aligned} \tag{2.13}$$

546 introducing in this way four gauge fields, $W_\mu^i(x)$ and $B_\mu(x)$, in the process. The
547 covariant derivatives (eqn 2.13) are required to transform in the same way as fermion
548 fields $\psi_i(x)$ themselves, therefore, the gauge fields transform as:

$$\begin{aligned}
B_\mu(x) &\xrightarrow{G} B'_\mu(x) \equiv B_\mu(x) - \frac{1}{g'} \partial_\mu \beta(x) \\
W_\mu^i(x) &\xrightarrow{G} W_\mu^{i'}(x) \equiv W_\mu^i(x) - \frac{i}{g} \partial_\mu \alpha_i(x) - \varepsilon_{ijk} \alpha_i(x) W_\mu^j(x).
\end{aligned} \tag{2.14}$$

549 The G invariant version of the Lagrangian density 2.9 can be written as

$$\mathcal{L}_0 = \sum_{j=1}^3 i\bar{\psi}_j(x) \gamma^\mu D_\mu \psi_j(x) \tag{2.15}$$

550 where free massless fermion and gauge fields and fermion-gauge boson interactions
551 are included. The EWI Lagrangian density must additionally include kinetic terms
552 for the gauge fields (\mathcal{L}_G) which are built from the field strengths, according to

$$B_{\mu\nu}(x) \equiv \partial_\mu B_\nu - \partial_\nu B_\mu \tag{2.16}$$

$$W_{\mu\nu}^i(x) \equiv \partial_\mu W_\nu^i(x) - \partial_\nu W_\mu^i(x) - g\varepsilon^{ijk} W_\mu^j W_\nu^k \tag{2.17}$$

553 the last term in eqn. 2.17 is added in order to hold the gauge invariance; therefore,

$$\mathcal{L}_G = -\frac{1}{4}B_{\mu\nu}(x)B^{\mu\nu}(x) - \frac{1}{4}W_{\mu\nu}^i(x)W_i^{\mu\nu}(x) \quad (2.18)$$

554 which contains not only the free gauge fields contributions but also the gauge fields
 555 self-interactions and interactions among them.

556 The three weak isospin conserved currents resulting from the $SU(2)_L$ symmetry are
 557 given by

$$J_\mu^i(x) = \frac{1}{2}\bar{\psi}_1(x)\gamma_\mu\sigma^i\psi_1(x) \quad (2.19)$$

558 while the weak hypercharge conserved current resulting from the $U(1)_Y$ symmetry is
 559 given by

$$J_\mu^Y = \sum_{j=1}^3 \bar{\psi}_j(x)\gamma_\mu y_j\psi_j(x) \quad (2.20)$$

560 In order to evaluate the electroweak interactions modeled by an isovector field W_μ^i
 561 which couples to isospin currents J_μ^i with strength g and additionally the singlet
 562 field B_μ which couples to the weak hypercharge current J_μ^Y with strength $g'/2$, the
 563 interaction Lagrangian density to be considered is

$$\mathcal{L}_I = -g J^{i\mu}(x) W_\mu^i(x) - \frac{g'}{2} J^Y{}^\mu(x) B_\mu(x) \quad (2.21)$$

564 Note that the weak isospin currents are not the same as the charged fermionic currents
 565 that were used to describe the WI (eqn 2.8), since the weak isospin eigenstates are
 566 not the same as the mass eigenstates, but they are closely related

$$J_\mu = \frac{1}{2}(J_\mu^1 + iJ_\mu^2), \quad J_\mu^\dagger = \frac{1}{2}(J_\mu^1 - iJ_\mu^2). \quad (2.22)$$

567 The same happen with the gauge fields W_μ^i which are related to the mass eigenstates
 568 W^\pm by

$$W_\mu^+ = \frac{1}{\sqrt{2}}(W_\mu^1 - iW_\mu^2), \quad W_\mu^- = \frac{1}{\sqrt{2}}(W_\mu^1 + iW_\mu^2). \quad (2.23)$$

569 The fact that there are three weak isospin conserved currents is an indication that in
 570 addition to the charged fermionic currents which couple charged to neutral leptons
 571 there should be a neutral fermionic current that couples neutral fermions or electri-
 572 cally charged fermions that has the same electric charge and thus does not imply
 573 electric charge change. The third weak isospin current contains a term that is simi-
 574 lar to the electromagnetic current (j_μ^{em}), indicating that there is a relation between
 575 them and resembling the Gell-Mann-Nishijima formula 2.3 adapted to electroweak
 576 interactions

$$Q = T_3 + \frac{Y_W}{2}. \quad (2.24)$$

577 Just as Q generates the $U(1)_{em}$ symmetry, the weak hypercharge generates the $U(1)_Y$
 578 symmetry as said before. It is possible to write the relationship in terms of the currents
 579 as

$$j_\mu^{em} = J_\mu^3 + \frac{1}{2}J_\mu^Y. \quad (2.25)$$

580 The neutral gauge fields W_μ^3 and B_μ cannot be directly identified with the Z and the
 581 photon fields since the photon interacts similarly with left and right-handed fermions;
 582 however, they are related through a linear combination given by

$$A_\mu = B_\mu \cos \theta_W + W_\mu^3 \sin \theta_W \quad (2.26)$$

$$Z_\mu = -B_\mu \sin \theta_W + W_\mu^3 \cos \theta_W$$

583 where θ_W is known as the “Weinberg angle.” The interaction Lagrangian is now given

584 by

$$\mathcal{L}_I = -\frac{g}{\sqrt{2}}(J^\mu W_\mu^+ + J^{\mu\dagger} W_\mu^-) - \left(g \sin \theta_W J_\mu^3 + g' \cos \theta_W \frac{J_\mu^Y}{2}\right) A^\mu - \left(g \cos \theta_W J_\mu^3 - g' \sin \theta_W \frac{J_\mu^Y}{2}\right) Z^\mu \quad (2.27)$$

585 the first term is the weak charged current interaction, while the second term is the

586 electromagnetic interaction under the condition

$$g \sin \theta_W = g' \cos \theta_W = e, \quad \frac{g'}{g} = \tan \theta_W \quad (2.28)$$

587 contained in the eqn.2.25; the third term is the neutral weak current.

588 Note that the neutral fields transformation given by the eqn. 2.26 can be written in

589 terms of the coupling constants g and g' as:

$$A_\mu = \frac{g' W_\mu^3 + g B_\mu}{\sqrt{g^2 + g'^2}}, \quad Z_\mu = \frac{g W_\mu^3 - g' B_\mu}{\sqrt{g^2 + g'^2}} \quad (2.29)$$

590 So far, the Lagrangian density describing the non-massive EWI is:

$$\mathcal{L}_{nmEWI} = \mathcal{L}_0 + \mathcal{L}_G \quad (2.30)$$

591 where fermion and gauge fields have been considered massless because their regular

592 mass terms are manifestly non invariant under G transformations; therefore, masses

593 have to be generated in a gauge invariant way. The mechanism by which this goal is

594 achieved is known as the “Higgs mechanism” and is closely connected to the concept
 595 of “spontaneous symmetry breaking.”

596 2.3.1 Spontaneous symmetry breaking

597 Figure 2.6 left shows a steel nail (top) which is subject to an external force; the form
 of the potential energy is also shown (bottom).

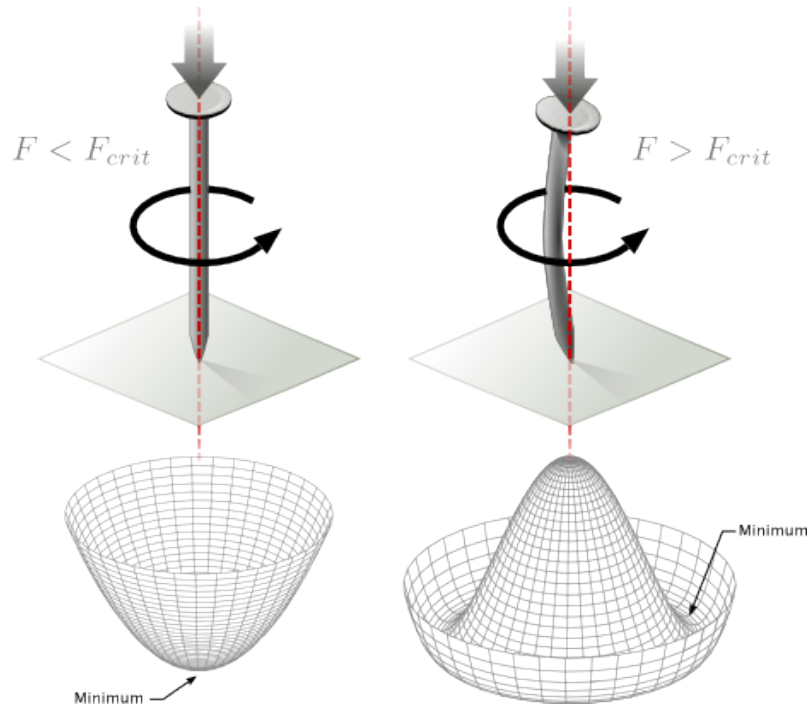


Figure 2.6: Spontaneous symmetry breaking mechanism. The steel nail, subject to an external force (top left), has rotational symmetry with respect to its axis. When the external force overcomes a critical value the nail buckles (top right) choosing a minimal energy state (ground state) and thus “*breaking spontaneously the rotational symmetry*”. The potential energy (bottom) changes but holds the rotational symmetry; however, an infinite number of asymmetric ground states are generated and circularly distributed in the bottom of the potential [34].

598
 599 Before reaching the critical force value, the system has rotational symmetry with re-
 600 spect to the nail axis; however, after the critical force value is reached the nail buckles
 601 (top right). The form of the potential energy (bottom right) changes, preserving its

602 rotational symmetry although its minima do not exhibit that rotational symmetry
 603 any longer. Right before the nail buckles there is no indication of the direction the
 604 nail will bend because any of the directions are equivalent, but once the nail bent,
 605 choosing a direction, an arbitrary minimal energy state (ground state) is selected and
 606 it does not share the system rotational symmetry. This mechanism for reaching an
 607 asymmetric ground state is known as “*spontaneous symmetry breaking (SSB)*”.
 608 The lesson from this analysis is that the way to introduce the SSB mechanism into a
 609 system is by adding the appropriate potential to it.

610

611 Figure 2.7 shows a plot of the potential $V(\phi)$ in the case of a scalar field ϕ

$$V(\phi) = \mu^2 \phi^\dagger \phi + \lambda (\phi^\dagger \phi)^2 \quad (2.31)$$

612 If $\mu^2 > 0$ the potential has only one minimum at $\phi = 0$ and describe a scalar field
 613 with mass μ . If $\mu^2 < 0$ the potential has a local maximum at $\phi = 0$ and two minima
 614 at $\phi = \pm\sqrt{-\mu^2/\lambda}$ which enables the SSB mechanism to work.

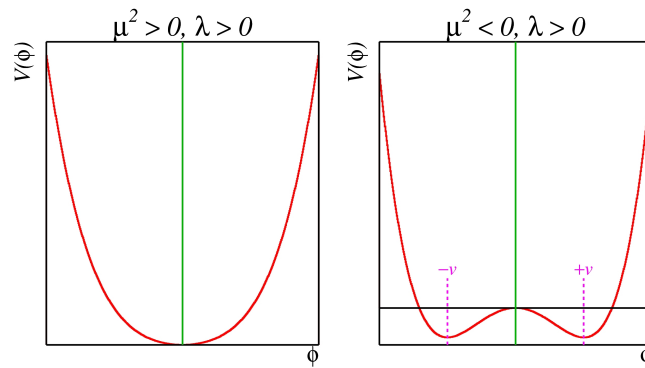


Figure 2.7: Shape of the potential $V(\phi)$ for $\lambda > 0$ and: $\mu^2 > 0$ (left) and $\mu^2 < 0$ (right). The case $\mu^2 < 0$ corresponds to the potential suitable for introducing the SSB mechanism by choosing one of the two ground states which are connected via reflection symmetry. [34].

615 In the case of a complex scalar field $\phi(x)$

$$\phi(x) = \frac{1}{\sqrt{2}}(\phi_1 + i\phi_2) \quad (2.32)$$

the Lagrangian (invariant under global $U(1)$ transformations) is given by

$$\mathcal{L} = (\partial_\mu \phi)^\dagger (\partial^\mu \phi) - V(\phi), \quad V(\phi) = \mu^2 \phi^\dagger \phi + \lambda (\phi^\dagger \phi)^2 \quad (2.33)$$

where an appropriate potential has been added in order to introduce the SSB.

As seen in figure 2.8, the potential has now an infinite number of minima circularly distributed along the ξ -direction which makes possible the occurrence of the SSB by choosing an arbitrary ground state; for instance, $\xi = 0$, i.e. $\phi_1 = v, \phi_2 = 0$

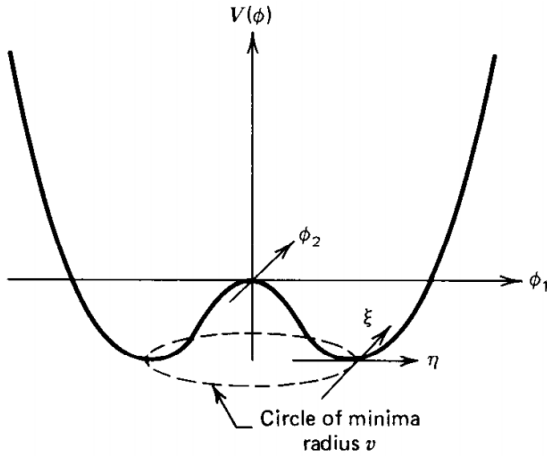


Figure 2.8: Potential for complex scalar field. There is a circle of minima of radius v along the ξ -direction [3].

$$\phi_0 = \frac{v}{\sqrt{2}} \exp(i\xi) \xrightarrow{\text{SSB}} \phi_0 = \frac{v}{\sqrt{2}} \quad (2.34)$$

As usual, excitations over the ground state are studied by making an expansion about it; thus, the excitation can be parametrized as:

$$\phi(x) = \frac{1}{\sqrt{2}}(v + \eta(x) + i\xi(x)) \quad (2.35)$$

623 which when substituted into eqn. 2.33 produces a Lagrangian in terms of the new
 624 fields η and ξ

$$\mathcal{L}' = \frac{1}{2}(\partial_\mu \xi)^2 + \frac{1}{2}(\partial_\mu \eta)^2 + \mu^2 \eta^2 - V(\phi_0) - \lambda v \eta (\eta^2 + \xi^2) - \frac{\lambda}{4}(\eta^2 + \xi^2)^2 \quad (2.36)$$

625 where the last two terms represent the interactions and self-interaction between the
 626 two fields η and ξ . The particular feature of the SSB mechanism is revealed when
 627 looking to the first three terms of \mathcal{L}' . Before the SSB, only the massless ϕ field is
 628 present in the system; after the SSB there are two fields of which the η -field has
 629 acquired mass $m_\eta = \sqrt{-2\mu^2}$ while the ξ -field is still massless (see figure 2.9).

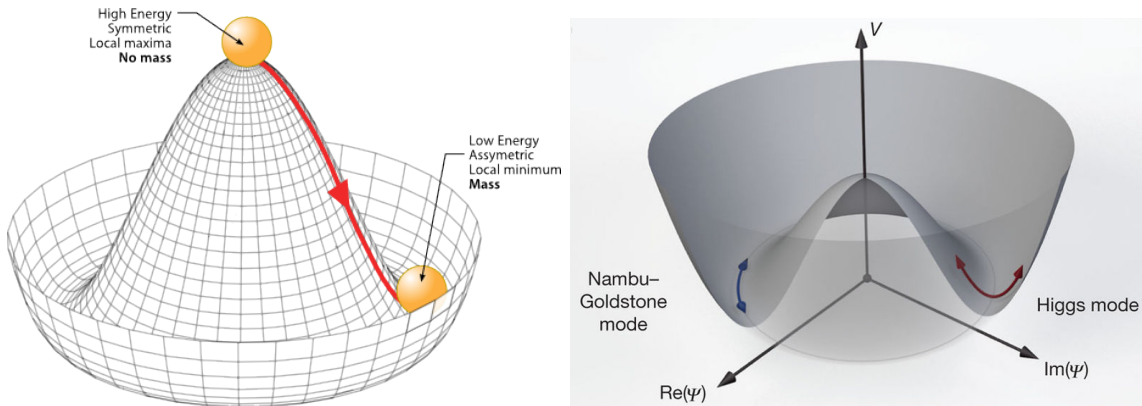


Figure 2.9: SSB mechanism for a complex scalar field [34, 35].

630 Thus, the SSB mechanism serves as a method to generate mass but as a side effect a
 631 massless field is introduced in the system. This fact is known as the Goldstone theorem
 632 and states that a massless scalar field appears in the system for each continuous
 633 symmetry spontaneously broken. Another version of the Goldstone theorem states
 634 that “if a Lagrangian is invariant under a continuous symmetry group G , but the
 635 vacuum is only invariant under a subgroup $H \subset G$, then there must exist as many
 636 massless spin-0 particles (Nambu-Goldstone bosons) as broken generators.” [33] The

637 Nambu-Goldstone boson can be understood considering that the potential in the ξ -
 638 direction is flat so excitations in that direction are not energy consuming and thus
 639 represent a massless state.

640 2.3.2 Higgs mechanism

641 When the SSB mechanism is introduced in the formulation of the EWI in an attempt
 642 to generate the mass of the so far massless gauge bosons and fermions, an interesting
 643 effect is revealed. In order to keep the G symmetry group invariance and generate
 644 the mass of the EW gauge bosons a G invariant Lagrangian density (\mathcal{L}_S) has to be
 645 added to the non massive EWI Lagrangian (eqn. 2.30)

$$\mathcal{L}_S = (D_\mu \phi)^\dagger (D^\mu \phi) - \mu^2 \phi^\dagger \phi - \lambda (\phi^\dagger \phi)^2, \quad \lambda > 0, \mu^2 < 0 \quad (2.37)$$

$$D_\mu \phi = \left(i\partial_\mu - g \frac{\sigma_i}{2} W_\mu^i - g' \frac{Y}{2} B_\mu \right) \phi \quad (2.38)$$

646 ϕ has to be an isospin doublet of complex scalar fields so it preserves the G invariance;
 647 thus ϕ can be defined as:

$$\phi = \begin{pmatrix} \phi^+ \\ \phi^0 \end{pmatrix} \equiv \frac{1}{\sqrt{2}} \begin{pmatrix} \phi_1 + i\phi_2 \\ \phi_3 + i\phi_4 \end{pmatrix}. \quad (2.39)$$

648 The minima of the potential are defined by

$$\phi^\dagger \phi = \frac{1}{2} (\phi_1^2 + \phi_2^2 + \phi_3^2 + \phi_4^2) = -\frac{\mu^2}{2\lambda}. \quad (2.40)$$

649 The choice of the ground state is critical. By choosing a ground state, invariant under
 650 $U(1)_{em}$ gauge symmetry, the photon will remain massless and the W^\pm and Z bosons
 651 masses will be generated which is exactly what is needed. In that sense, the best

652 choice corresponds to a weak isospin doublet with $T_3 = -1/2$, $Y_W = 1$ and $Q = 0$
 653 which defines a ground state with $\phi_1 = \phi_2 = \phi_4$ and $\phi_3 = v$:

$$\phi_0 \equiv \frac{1}{\sqrt{2}} \begin{pmatrix} 0 \\ v \end{pmatrix}, \quad v^2 \equiv -\frac{\mu^2}{\lambda}. \quad (2.41)$$

654 where the vacuum expectation value v is fixed by the Fermi coupling G_F according
 655 to $v = (\sqrt{2}G_F)^{1/2} \approx 246$ GeV.

656 The G symmetry has been broken and three Nambu-Goldstone bosons will appear.
 657 The next step is to expand ϕ about the chosen ground state as:

$$\phi(x) = \frac{1}{\sqrt{2}} \exp\left(\frac{i}{v} \sigma_i \theta^i(x)\right) \begin{pmatrix} 0 \\ v + H(x) \end{pmatrix} \approx \frac{1}{\sqrt{2}} \begin{pmatrix} \theta_1(x) + i\theta_2(x) \\ v + H(x) - i\theta_3(x) \end{pmatrix} \quad (2.42)$$

658 to describe fluctuations from the ground state ϕ_0 . The fields $\theta_i(x)$ represent the
 659 Nambu-Goldstone bosons while $H(x)$ is known as “higgs field.” The fundamental
 660 feature of the parametrization used is that the dependence on the $\theta_i(x)$ fields is
 661 factored out in a global phase that can be eliminated by taking the physical “unitary
 662 gauge” $\theta_i(x) = 0$. Therefore the expansion about the ground state is given by:

$$\phi(x) \frac{1}{\sqrt{2}} \begin{pmatrix} 0 \\ v + H(x) \end{pmatrix} \quad (2.43)$$

663 which when substituted into \mathcal{L}_S (eqn. 2.37) results in a Lagrangian containing the now
 664 massive three gauge bosons W^\pm, Z , one massless gauge boson (photon) and the new
 665 Higgs field (H). The three degrees of freedom corresponding to the Nambu-Goldstone
 666 bosons are now integrated into the massive gauge bosons as their longitudinal polar-
 667 izations which were not available when they were massless particles. The effect by
 668 which vector boson fields acquire mass after an spontaneous symmetry breaking but
 669 without an explicit gauge invariance breaking is known as the “*Higgs mechanism*.”

670 The mechanism was proposed by three independent groups: F.Englert and R.Brout
 671 in August 1964 [36], P.Higgs in October 1964 [37] and G.Guralnik, C.Hagen and
 672 T.Kibble in November 1964 [38]; however, its importance was not realized until
 673 S.Glashow [14], A.Salam [15] and S.Weinberg [16] independently proposed that elec-
 674 tromagnetic and weak interactions are two manifestations of a more general interac-
 675 tion called “electroweak interaction” in 1967.

676 2.3.3 Masses of the gauge bosons

677 The mass of the gauge bosons is extracted by evaluating the kinetic part of Lagrangian
 678 \mathcal{L}_S in the ground state (known also as the vacuum expectation value) i.e.

$$\left| \left(\partial_\mu - ig \frac{\sigma_i}{2} W_\mu^i - i \frac{g'}{2} B_\mu \right) \phi_0 \right|^2 = \left(\frac{1}{2} v g \right)^2 W_\mu^+ W^{-\mu} + \frac{1}{8} v^2 (W_\mu^3, B_\mu) \begin{pmatrix} g^2 & -gg' \\ -gg' & g'^2 \end{pmatrix} \begin{pmatrix} W^{3\mu} \\ B^\mu \end{pmatrix} \quad (2.44)$$

679 comparing with the typical mass term for a charged boson $M_W^2 W^+ W^-$

$$M_W = \frac{1}{2} v g. \quad (2.45)$$

The second term in the right side of the eqn.2.44 comprises the masses of the neutral
 bosons, but it needs to be written in terms of the gauge fields Z_μ and A_μ in order to
 be compared to the typical mass terms for neutral bosons, therefore using eqn. 2.29

$$\begin{aligned} \frac{1}{8} v^2 [g^2 (W_\mu^3)^2 - 2gg' W_\mu^3 B^\mu + g'^2 B_\mu^2] &= \frac{1}{8} v^2 [g W_\mu^3 - g' B_\mu]^2 + 0[g' W_\mu^3 + g B_\mu]^2 \quad (2.46) \\ &= \frac{1}{8} v^2 [\sqrt{g^2 + g'^2} Z_\mu]^2 + 0[\sqrt{g^2 + g'^2} A_\mu]^2 \end{aligned}$$

680 and then

$$M_Z = \frac{1}{2}v\sqrt{g^2 + g'^2}, \quad M_A = 0 \quad (2.47)$$

681 2.3.4 Masses of the fermions

682 The lepton mass terms can be generated by introducing a gauge invariant Lagrangian
 683 term describing the Yukawa coupling between the lepton field and the Higgs field:

$$\mathcal{L}_{Yl} = -G_l \left[(\bar{\nu}_l, \bar{l})_L \begin{pmatrix} \phi^+ \\ \phi^0 \end{pmatrix} l_R + \bar{l}_R (\phi^-, \bar{\phi}^0) \begin{pmatrix} \nu_l \\ l \end{pmatrix} \right], \quad l = e, \mu, \tau. \quad (2.48)$$

684 After the SSB and replacing the usual field expansion about the ground state (eqn.2.41)
 685 into \mathcal{L}_{Yl} , the mass term arises

$$\mathcal{L}_{Yl} = -m_l(\bar{l}_L l_R + \bar{l}_R l_L) - \frac{m_l}{v}(\bar{l}_L l_R + \bar{l}_R l_L)H = -m_l \bar{l}l \left(1 + \frac{H}{v}\right) \quad (2.49)$$

686

$$m_l = \frac{G_l}{\sqrt{2}}v \quad (2.50)$$

687 where the additional term represents the lepton-Higgs interaction. The quark masses
 688 are generated in a similar way as lepton masses but for the upper member of the
 689 quark doublet a different Higgs doublet is needed:

$$\phi_c = -i\sigma_2\phi^* = \begin{pmatrix} -\bar{\phi}^0 \\ \phi^- \end{pmatrix}. \quad (2.51)$$

690 Additionally, given that the quark isospin doublets are not constructed in terms of
 691 the mass eigenstates but in terms of the flavor eigenstates as shown in table2.4, the
 692 coupling parameters will be related to the CKM matrix elements; thus the quark
 693 Lagrangian is given by:

$$\mathcal{L}_{Yq} = -G_d^{i,j}(\bar{u}_i, \bar{d}'_i)_L \begin{pmatrix} \phi^+ \\ \phi^0 \end{pmatrix} d_{jR} - G_u^{i,j}(\bar{u}_i, \bar{d}'_i)_L \begin{pmatrix} -\bar{\phi}^0 \\ \phi^- \end{pmatrix} u_{jR} + h.c. \quad (2.52)$$

with $i,j=1,2,3$. After SSB and expansion about the ground state, the diagonal form of \mathcal{L}_{Yq} is:

$$\mathcal{L}_{Yq} = -m_d^i \bar{d}_i d_i \left(1 + \frac{H}{v}\right) - m_u^i \bar{u}_i u_i \left(1 + \frac{H}{v}\right) \quad (2.53)$$

Fermion masses depends on arbitrary couplings G_l and $G_{u,d}$ and are not predicted by the theory.

2.3.5 The Higgs field

After the characterization of the fermions and gauge bosons as well as their interactions, it is necessary to characterize the Higgs field itself. The Lagrangian \mathcal{L}_S in eqn:2.37 written in terms of the gauge bosons is given by

$$\mathcal{L}_S = \frac{1}{4} \lambda v^4 + \mathcal{L}_H + \mathcal{L}_{HV} \quad (2.54)$$

$$\mathcal{L}_H = \frac{1}{2} \partial_\mu H \partial^\mu H - \frac{1}{2} m_H^2 H^2 - \frac{1}{2v} m_H^2 H^3 - \frac{1}{8v^2} m_H^2 H^4 \quad (2.55)$$

$$\mathcal{L}_{HV} = m_H^2 W_\mu^+ W^{\mu-} \left(1 + \frac{2}{v} H + \frac{2}{v^2} H^2\right) + \frac{1}{2} m_Z^2 Z_\mu Z^\mu \left(1 + \frac{2}{v} H + \frac{2}{v^2} H^2\right) \quad (2.56)$$

The mass of the Higgs boson is deduced as usual from the mass term in the Lagrangian resulting in:

$$m_H = \sqrt{-2\mu^2} = \sqrt{2\lambda}v \quad (2.57)$$

however, it too is not predicted by the theory. The experimental efforts to find the Higgs boson, carried out by the CMS and ATLAS experiments⁸, gave great results

⁸ CMS stands for Compact Muon Solenoid; ATLAS stand for A Toroidal LHC Apparatus. Both are general experiments held at the Large Hadron Collider(LHC)

708 by July of 2012 when the discovery of a new particles was announced and which
 709 is compatible with the Higgs boson predicted by the electroweak theory [39, 40].
 710 Although at the announcement time there were some reservations about calling the
 711 new particle the “Higgs boson”, today this name is widely accepted. The result of
 712 the measurement of the Higgs mass reported by both experiments [41] is in table 2.7.

Property	Value
Electric charge	0
Colour charge	0
Spin	0
Weak isospin	-1/2
Weak hypercharge	1
Parity	1
Mass (GeV/c^2)	$125.09 \pm 0.21 \text{ (stat.)} \pm 0.11 \text{ (syst.)}$

Table 2.7: Higgs boson properties. Higgs mass is not predicted by the theory and the value here corresponds to the experimental measurement.

713

714 2.3.6 Higgs boson production mechanisms at LHC.

715 At LHC, Higgs boson is produced as a result of the collision of two counter-rotating
 716 protons beams. A detailed description of the LHC machine will be presented in the
 717 chapter 3. “The total cross section” is the parameter that quantify the number of pp
 718 collisions that happen when a number of protons are fired at each other. Different
 719 results can be obtained after a pp collision and for each one the “cross section” is
 720 defined as the number of pp collisions that conclude in that particular result with
 721 respect to the number of protons fired at each other.

722 Protons are composed of quarks and these quarks are bound by gluons; however, what
 723 is commonly called the quark content of the proton makes reference to the valence
 724 quarks. A sea of quarks and gluons is also present inside the proton as represented
 725 in figure 2.10. In a proton-proton (pp) collision, the constituents (quarks and gluons)

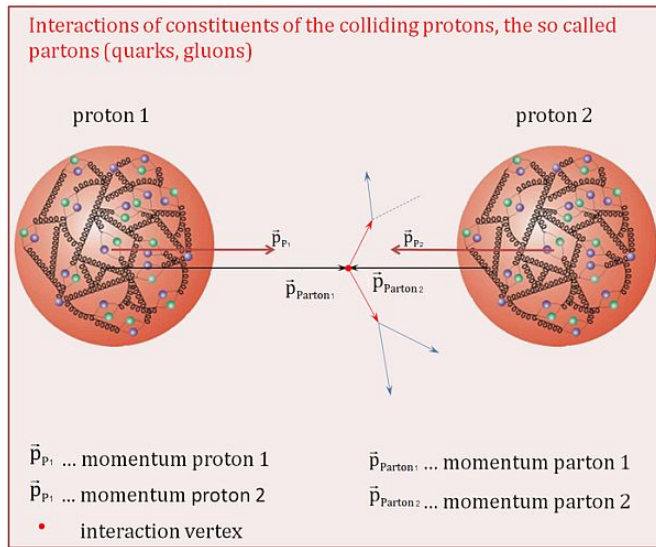


Figure 2.10: Proton-proton collision. Protons are composed of 3 valence quarks, a sea of quarks and gluons; therefore in a proton-proton collision, quarks and gluons are those who collide. [45].

are those who collide. The pp cross section depends on the momentum of the colliding particles, reason for which it is needed to know how the momentum is distributed inside the proton. Quarks and gluons are known as partons and the functions that describes how the proton momentum is distributed among partons inside it are called “parton distribution functions (PDFs)”; PDFs are determined from experimental data obtained in experiments where the internal structure of hadrons is tested.

In addition, in physics, a common approach to study complex systems consist in starting with a simpler version of them, for which a well known description is available, and add an additional “perturbation” which represent a small deviation from the known behavior. If the perturbation is small enough, the physical quantities associated with the perturbed system are expressed as a series of corrections to those of the simpler system; therefore, the more terms are considered in the series (the higher order in the perturbation series), the more precise is the the description of the complex system.

740 This thesis explore the Higgs production at LHC; therefore the overview presented
 741 here will be oriented specifically to the production mechanisms after pp collisions at
 742 LHC.

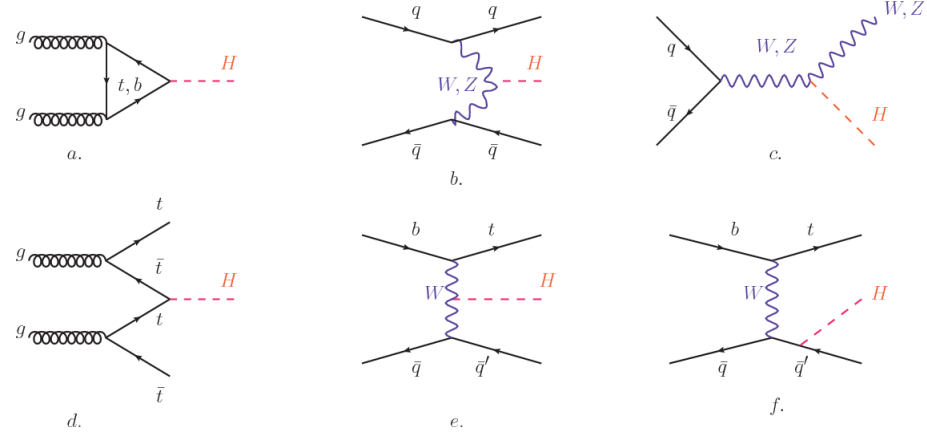


Figure 2.11: Main Higgs production mechanism Feynman diagrams. a. gluon-gluon fusion, b. vector boson fusion (VBF), c. Higgs-strahlung, d. Associated production with a top or bottom quark pair, e-f. associated production with a single top quark.

743 Figure 2.11 shows the Feynman diagrams for the leading order (first order) Higgs
 744 production processes at LHC, while the cross section for Higgs production as a func-
 745 tion of the center of mass-energy (\sqrt{s}) for pp collisions is showed in figure 2.12 left.
 746 The tags NLO (next to leading order), NNLO (next to next to leading order) and
 747 N3LO (next to next to next to leading order) make reference to the order at which
 748 the perturbation series has been considered.

749 As shown in eqns 2.48, 2.52 and 2.56, the strength of the Higgs-fermion interaction
 750 is proportional to the fermion mass while the strength of the Higgs-gauge boson
 751 interaction is proportional to the square of the gauge boson mass, which implies
 752 that the Higgs production and decay mechanisms are dominated by couplings $H -$
 753 (W, Z, t, b, τ) .

754 The main production mechanism is the gluon fusion (figure 2.11a and $pp \rightarrow H$ in figure
 755 2.12) given that gluons carry the highest fraction of momentum of the protons in pp

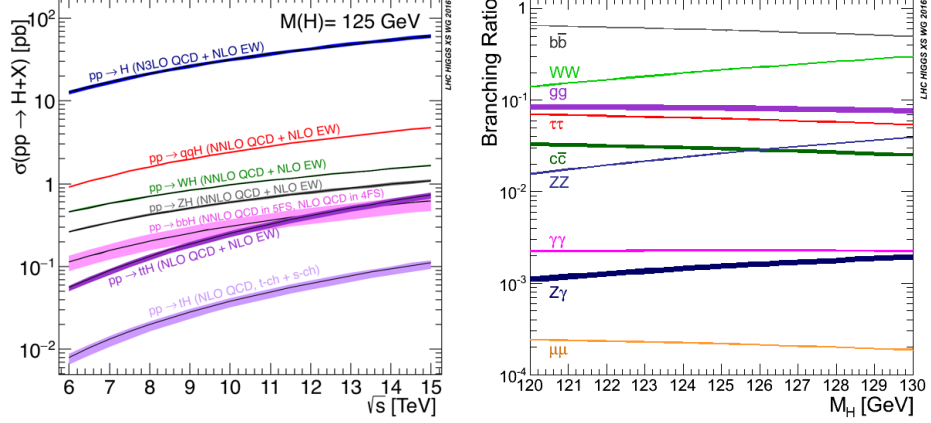


Figure 2.12: Higgs production cross sections (left) and decay branching ratios (right) for the main mechanisms. The VBF is indicated as qqH [42].

colliders. Since the Higgs boson does not couple to gluons, the mechanism proceeds through the exchange of a virtual top-quark loop given that for it the coupling is the biggest. Note that in this process, the Higgs boson is produced alone, which makes this mechanism experimentally clean when combined with the two-photon or the four-lepton decay channels (see section 2.3.7).

Vector boson fusion (figure 2.11b and $pp \rightarrow qqH$ in figure 2.12) has the second largest production cross section. The scattering of two fermions is mediated by a weak gauge boson which later emits a Higgs boson. In the final state, the two fermions tend to be located in a particular region of the detector which is used as a signature when analyzing the datasets provided by the experiments. More details about how to identify events of interest in an analysis will be given in chapter 4.

The next production mechanism is Higgs-strahlung (figure 2.11c and $pp \rightarrow WH, pp \rightarrow ZH$ in figure 2.12) where two fermions annihilate to form a weak gauge boson. If the initial fermions have enough energy, the emergent boson eventually will emit a Higgs boson.

The associated production with a top or bottom quark pair and the associated pro-

duction with a single top quark (figure 2.11d-f and $pp \rightarrow bbH, pp \rightarrow t\bar{t}H, pp \rightarrow tH$ in figure 2.12) have a smaller cross section than the main three mechanisms above, but they provide a good opportunity to test the Higgs-top coupling. The analysis reported in this thesis is developed using these production mechanisms. A detailed description of the tH mechanism will be given in section 2.4.

2.3.7 Higgs decay channels

When a particle can decays through several modes, also known as channels, the probability of decaying through a given channel is quantified by the “branching ratio (BR)” of the decay channel; thus, the BR is defined as the ratio of number of decays going through that given channel to the total number of decays. In regard to the Higgs boson decay, the BR can be predicted with accuracy once the Higgs mass is known [43, 44]. In figure 2.12 right, a plot of the BR as a function of the Higgs mass is presented. The largest predicted BR corresponds to the $b\bar{b}$ pair decay channel (see table 2.8).

Decay channel	Branching ratio	Rel. uncertainty
$H \rightarrow b\bar{b}$	5.84×10^{-1}	$+3.2\% - 3.3\%$
$H \rightarrow W^+W^-$	2.14×10^{-1}	$+4.3\% - 4.2\%$
$H \rightarrow \tau^+\tau^-$	6.27×10^{-2}	$+5.7\% - 5.7\%$
$H \rightarrow ZZ$	2.62×10^{-2}	$+4.3\% - 4.1\%$
$H \rightarrow \gamma\gamma$	2.27×10^{-3}	$+5.0\% - 4.9\%$
$H \rightarrow Z\gamma$	1.53×10^{-3}	$+9.0\% - 8.9\%$
$H \rightarrow \mu^+\mu^-$	2.18×10^{-4}	$+6.0\% - 5.9\%$

Table 2.8: Predicted branching ratios and the relative uncertainty for a SM Higgs boson with $m_H = 125\text{GeV}/c^2$. [21]

787 **2.4 Associated Production of Higgs Boson and**
 788 **Single Top Quark.**

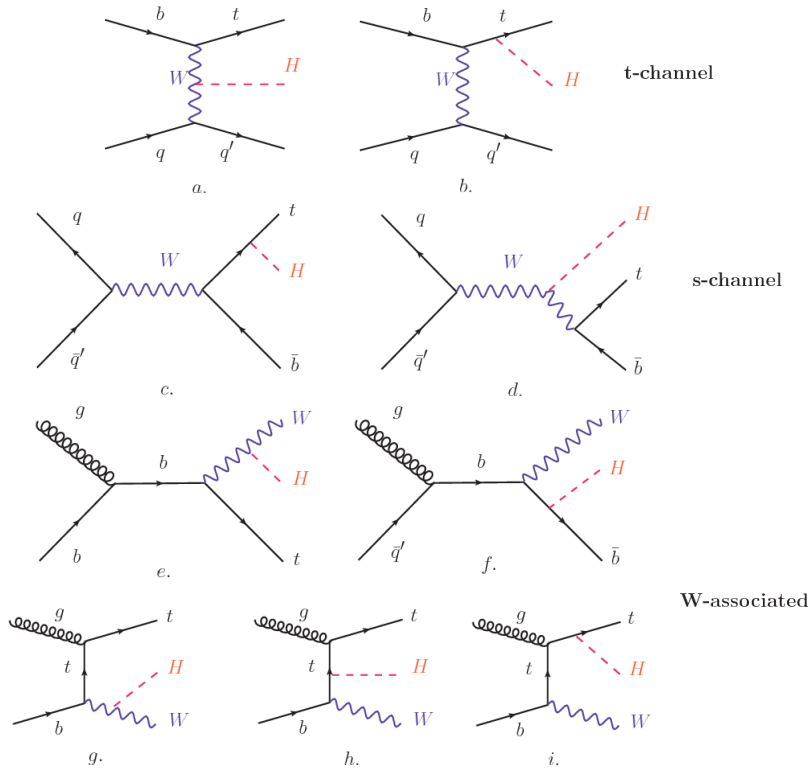


Figure 2.13: Associated higgs production mechanism Feynman diagrams. a.,b. t-channel (tHq), c.,d. s-channel (tHb), e-i. W-associated.

789 Associated production of Higgs boson have been extensively studied [46–50]. While
 790 measurements of the main Higgs production mechanisms rates are sensitive to the
 791 strength of the Higgs coupling to W boson or top quark, they are not sensitive to the
 792 relative sign between the two couplings. In this thesis, the Higgs boson production
 793 mechanism explored is the associated production with a single top quark (*th*) which
 794 offers sensitiveness to the relative sign of the Higgs couplings to W boson and to top
 795 quark. The description given here is based on the references [?, 48]

797 A process where two incoming particles interact and produce a final state with two
 798 particles can proceed in three ways also called channels (see, for instance, figure 2.13
 799 omitting the red line). The t-channel represents processes where an intermediate
 800 particle is emitted by one of the incoming particles and absorbed by the other. The
 801 s-channel represent processes where the two incoming particles merge into an inter-
 802 mediate particle which eventually will split into the particles in the final state. The
 803 third channel, u-channel, is similar to the t-channel but the two outgoing particles
 804 interchange their roles.

805

806 The tH production where Higgs boson can be radiated either from the top quark or
 807 from the W boson is represented by the leading order Feynman diagrams in figure
 808 2.13. The cross section for the tH process is calculated, as usual, summing over
 809 the contributions from the different feynman diagrams; therefore it depends on the
 810 interference between the contributions. In the SM, the interference for t-channel (tHq
 811 process) and W-associated (tHW process) production is destructive [46] resulting in
 812 the small cross sections presented in table 2.9.

tH production channel	Cross section (fb)
t-channel ($pp \rightarrow tHq$)	$70.79^{+2.99}_{-4.80}$
W-associated ($pp \rightarrow tHW$)	$15.61^{+0.83}_{-1.04}$
s-channel($pp \rightarrow tHb$)	$2.87^{+0.09}_{-0.08}$

Table 2.9: Predicted SM cross sections for tH production at $\sqrt{s} = 13$ TeV [51, 52].

813

814 While the s-channel contribution can be neglected, it will be shown that a deviation
 815 from the SM destructive interference would result in an enhancement of the tH cross
 816 section compared to that in SM, which could be used to get information about the

817 sign of the Higgs-top coupling [48, 49]. In order to describe th production processes,
 818 Feynman diagram 2.13b will be considered; there, the W boson is radiated by a
 819 quark in the proton and eventually it will interact with the b quark. In the high
 820 energy regime, the effective W approximation [53] allows to describe the process as
 821 the emmision of an approximately on-shell W and its hard scattering with the b
 822 quark; i.e. $Wb \rightarrow th$. The scattering amplitude for the process is given by

$$\mathcal{A} = \frac{g}{\sqrt{2}} \left[(C_t - C_V) \frac{m_t \sqrt{s}}{m_W v} A \left(\frac{t}{s}, \varphi; \xi_t, \xi_b \right) + \left(C_V \frac{2m_W s}{v} \frac{1}{t} + (2C_t - C_V) \frac{m_t^2}{m_W v} \right) B \left(\frac{t}{s}, \varphi; \xi_t, \xi_b \right) \right], \quad (2.58)$$

823 where $C_V \equiv g_{HVV}/g_{HVV}^{SM}$ and $C_t \equiv g_{Ht}/g_{Ht}^{SM}$ are scaling factors that quantify possible
 824 deviations of the couplings, Higgs-Vector boson (H-W) and Higgs-top (H-t) respec-
 825 tively, from the SM couplings; $s = (p_W + p_b)^2$, $t = (p_W - p_H)^2$, φ is the Higgs azimuthal
 826 angle around the z axis taken parallel to the direction of motion of the incoming W;
 827 A and B are funtions describing the weak interaction in terms of the chiral states of
 828 the quarks b and t. Terms that vanish in the high energy limit have been neglected
 829 as well as the Higgs and b quark masses⁹.

830

831 The scattering amplitude grows with energy like \sqrt{s} for $C_V \neq C_t$, in contract to
 832 the SM ($C_t = C_V = 1$) where the first term in 2.58 cancels out and the amplitude
 833 is constant for large s; therefore, a deviation from the SM predictions represent an
 834 enhancement in the th cross section. A simmilar analysis is valid for the W-associated
 835 channel but the interference is more complicated since there are more than two con-
 836 tributions. In particular, for a SM H-W coupling and a H-t coupling of inverted sigh
 837 with respect to the SM ($C_V = -C_t = 1$) the tHq cross section is enhanced by a factor

⁹ A detailed explanation of the structure and approximations used to derive \mathcal{A} can be fount in reference [48]

greater 10 as seen in the figure 2.14 taken from reference [48]; other study have reported similar enhancement results [54]. Results from both references are presented in table 2.10.

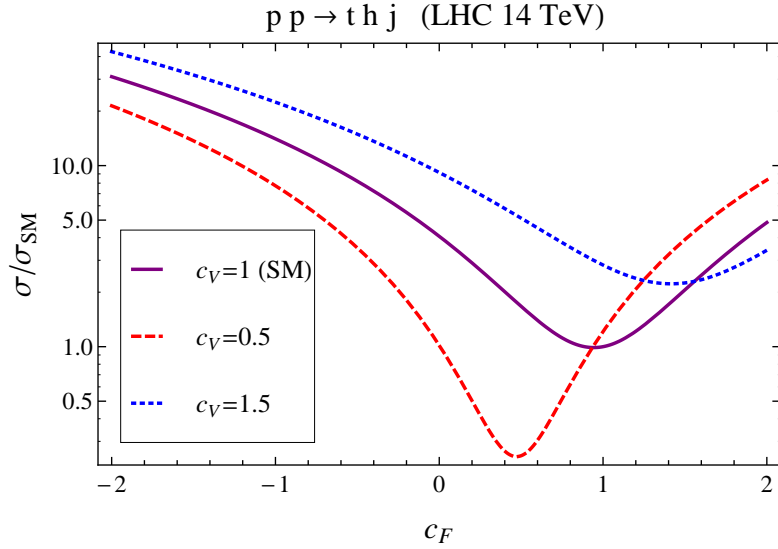


Figure 2.14: Cross section for tHq process as a function of C_t , normalized to the SM, for three values of C_V . In the plot C_f refers to the Higgs-fermion coupling which is dominated by the H-t coupling C_t . Solid, dashed and dotted lines correspond to $C_V = 1, 0.5, 1.5$ respectively. Note that for the SM ($C_V = C_t = 1$), the destructive effect of the interference is maximal.

	\sqrt{s} TeV	$C_t = 1$	$C_t = -1$
$\sigma^{LO}(tHq)(\text{fb})$ [48]	8	≈ 17.4	≈ 252.7
	14	≈ 80.4	≈ 1042
$\sigma^{NLO}(tHq)(\text{fb})$ [48]	8	$18.28^{+0.42}_{-0.38}$	$233.8^{+4.6}_{-0.0}$
	14	$88.2^{+1.7}_{-0.0}$	$982.8^{+28}_{-0.0}$
$\sigma^{LO}(tHq)(\text{fb})$ [54]	14	≈ 71.8	≈ 893
$\sigma^{LO}(tHW)(\text{fb})$ [54]	14	≈ 16.0	≈ 139

Table 2.10: Predicted enhancement of the tHq cross sections at LHC for $C_V = 1$ and $C_t = \pm 1$ at LO and NLO; the cross section enhancement of more than a factor of 10 is due to the flipping in the sign of the H-t coupling with respect to the SM one.

⁸⁴² 2.5 The CP-mixing phase

⁸⁴³ Chapter 3

⁸⁴⁴ The CMS experiment at the LHC

⁸⁴⁵ 3.1 Introduction

⁸⁴⁶ Located in the Swiss-French border, the European Council for Nuclear Research
⁸⁴⁷ (CERN) is the largest scientific organization leading the particle physics research.
⁸⁴⁸ About 13000 people in a broad range of fields including users, students, scientists,
⁸⁴⁹ engineers among others, contribute to the data taking and analysis, with the goal
⁸⁵⁰ of unveiling the secrets of the nature and revealing the fundamental structure of the
⁸⁵¹ universe. CERN is also the home of the Large Hadron Collider (LHC), the largest
⁸⁵² circular particle accelerator around the world, where protons (or heavy ions) traveling
⁸⁵³ close to the speed of light, are made to collide. These collisions open a window to
⁸⁵⁴ investigate how particles (and their constituents if they are composite) interact with
⁸⁵⁵ each other, providing clues about the laws of the nature.

⁸⁵⁶ LHC can run in three modes depending on the particles being accelerated

- ⁸⁵⁷ • Proton-Proton collisions (pp) multiple physics experiments .
- ⁸⁵⁸ • Lead-Lead collisions (Pb-Pb) Heavy ion experiments.

- 859 • Proton-Lead collisions (p-Pb).

860 Figure 3.1 show an overview of the CERN accelerating complex. There are several
 861 accelerating stages before the injection to the LHC ring. In the pp mode, after
 862 removing the electrons from hydrogen atoms in a bottle, protons are accelerated
 863 in the LINAC2 to 50 MeV and then injected into the proton synchrotron booster
 864 (BOOSTER) to reach 1.4 GeV in energy. The next boost is provided at the proton
 865 synchrotron (PS) up to 26 GeV, followed by the injection into the super proton
 866 synchrotron (SPS) where protons are accelerated to 450 GeV. Finally, protons are
 867 injected into the LHC where they are accelerated to the target energy of 6.5 TeV. In
 868 the Pb-Pb mode, the Lead ions are first accelerated in the LINAC3 and then passed as
 869 long pulses to the Low energy ion ring (LEIR) to be converted into short and dense
 870 bunches, each containing 7×10^7 lead ions. LEIR accelerate the bunches from 4.2
 871 MeV to 72 MeV. The ions are then passed to the PS to follow the rest of acceleration
 872 process up to 2.8TeV/n en the LHC ring.

873 **3.2 The LHC**

874 The LHC is a 27 km ring composed of superconducting magnets and accelerating
 875 structures (among other components) which boost the particles traveling inside it.
 876 It is installed in the same tunnel where the large Electron-Positron (LEP) collider
 877 was located, taking advantage of the existing infraestructure as shown in Figure 3.2.
 878 Two particle beams travel counter-rotating in two separated beam pipes kept at ultra
 879 high vacuum. In 2008, the first set of collisions involved protons with center-of-mass
 880 energy of 7 TeV after which the energy was increased to 8 TeV in 2012 and to 13 TeV
 881 in 2015.

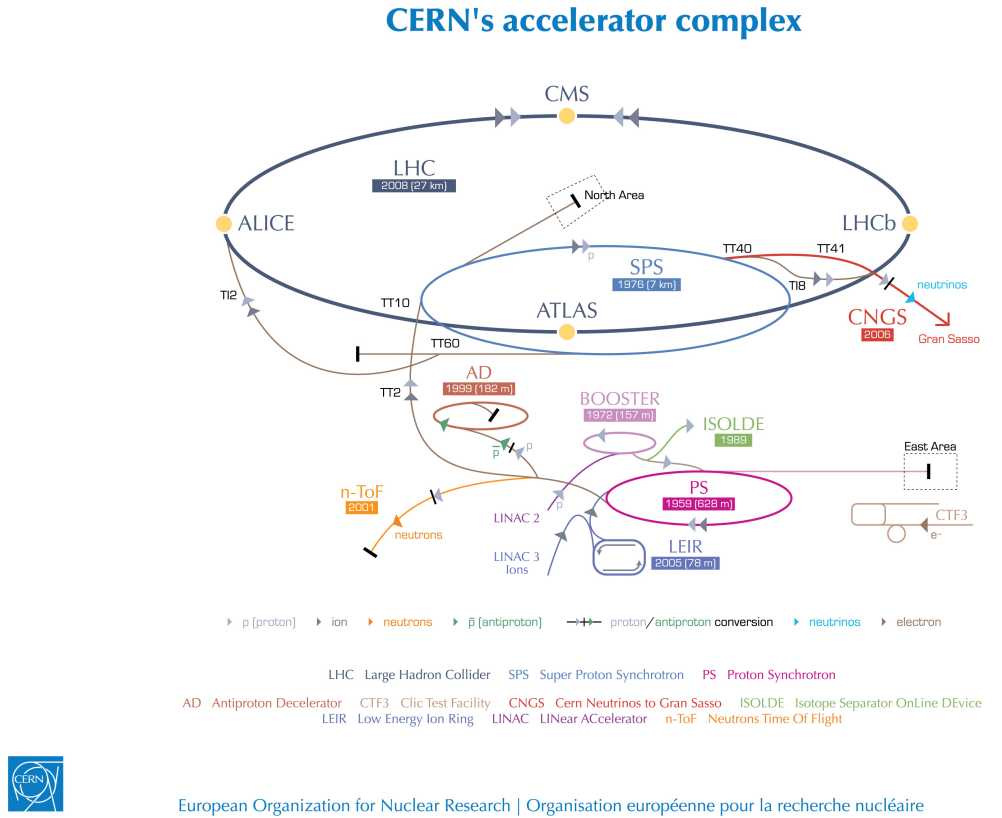
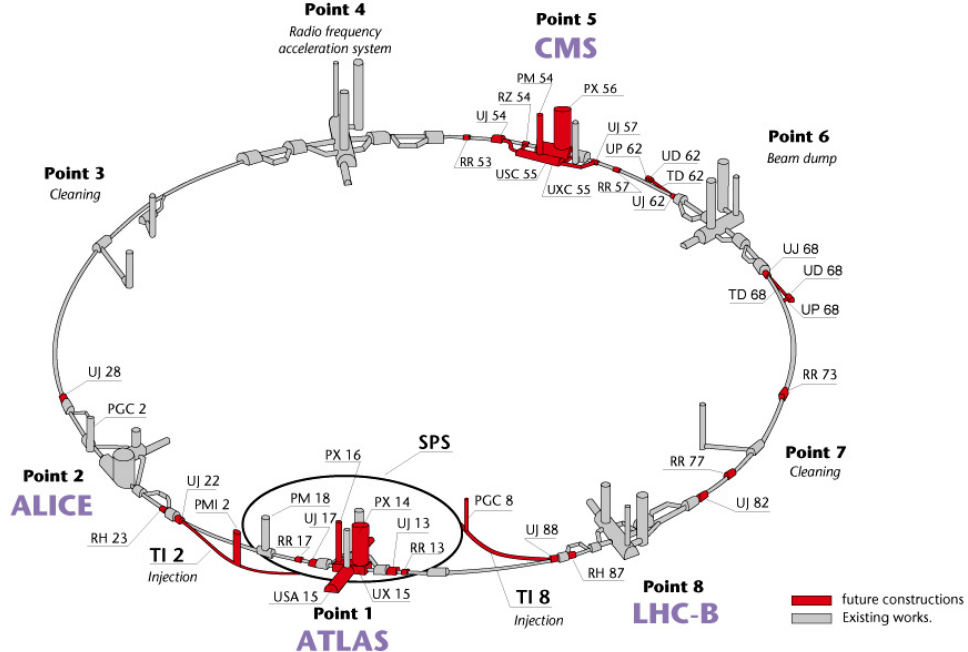


Figure 3.1: ref. C.Lefevre, “The CERN accelerator complex,” (2008). CERN-DI-0812015.

882 In order to keep the protons in the circular trajectory carrying that amount of
 883 energy, strong magnetic fields are needed, bringing the superconductivity into scene.
 884 The superconducting dipole magnets used in LHC are made of a NbTi alloy, capable
 885 of transporting currents of about 12000 A when cooled at a temperature below 2K by
 886 using liquid helium; that current generates a magnetic fields of 8.3 T. Figure 3.3 shows
 887 the transverse view of the LHC dipole magnets. Additionally, quadrupole magnets
 888 are used to focus the beam and some other magnetic multipoles are used to correct
 889 effects generated by the interaction among protons in the beam as well as interactions
 890 within the beam pipe.
 891 Regarding to the longitudinal acceleration of the protons, a system of 16 radio-
 892 frecuency cavities (RF) (8 per beam) is used to accelerate protons. Inside the cavities,

Layout of the LEP tunnel including future LHC infrastructures.



CERN AC _ hf238 _ V02/02/98

Figure 3.2: ref. J.-L. Caron , “Layout of the LEP tunnel including future LHC infrastructures.. L’ensemble du tunnel LEP avec les futures infrastructures LHC.”, <https://cds.cern.ch/record/841542> (Nov, 1993). AC Collection. Legacy of AC. Pictures from 1992 to 2002..

893 the electromagnetic waves become resonant transferring the maximum energy to the
 894 particle flight through it. Cavities are cooled at 4.5 K. On LHC the RF oscillation
 895 frecuency is 400MHz and the protons are carefully timed so additionally to the ac-
 896 celeration effect the bunch structure of the beam is preserved. The Beam is made
 897 of 2808 “bunches” which are packages of 1.15×10^{11} protons ???. If LHC is at full
 898 energy, protons with the right energy does not feel any accelerating force but those
 899 with a different energy will be accelerated or decelerated to keep them in the bunch.
 900 The paths followed by particles during the acceleration process are shown in Figure
 901 3.1.

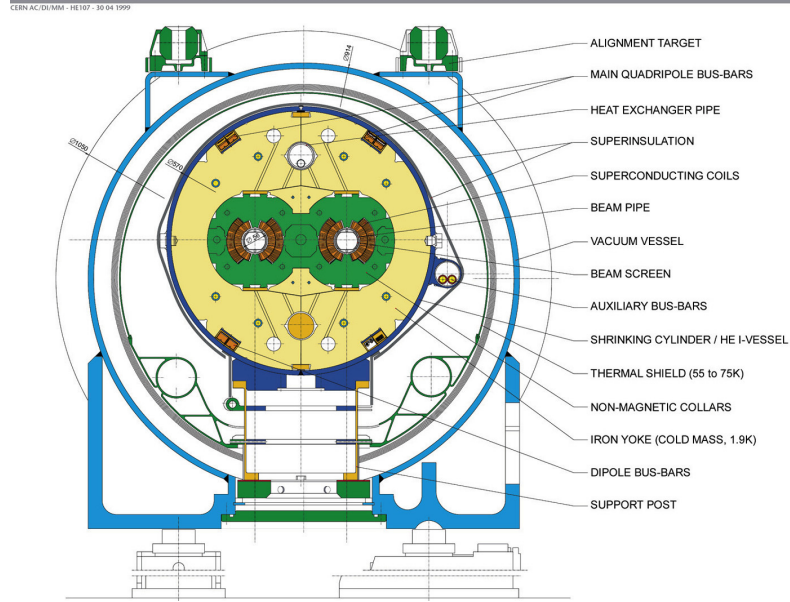
LHC DIPOLE : STANDARD CROSS-SECTION


Figure 3.3: ref. ACTeam, “Diagram of an LHC dipole magnet. Schéma d’un aimant dipôle du LHC,” (1999). CERN-DI-9906025.

902 Once the beams reach the desired energy, they are brought to cross each other
 903 producing proton-proton collisions. The bunch crossing happens in precise places
 904 where the LHC experiments are located. As seen in Figure 3.2, it was needed to
 905 build the caverns for CMS and ATLAS as well as some additional facilities, but
 906 most of the initial LEP infrastructure has been used to allocate additional collision
 907 points. The highest luminosity is delivered at the CMS (point 5) and ATLAS (point
 908 1) experiments, which are general purpose experiments, enabled to explore physics
 909 in any of the collision modes. LHCb (point 8) experiment is optimized to explore
 910 B-physics, while ALICE (point 2) is optimized for heavy ion collisions researches;
 911 TOTEM (point 5) and LHCf (point 1) are dedicated to forward physics studies and
 912 MoEDAL (point 8) is intended for monopoles or massive pseudo stable particles
 913 studies.

914 3.3 The CMS experiment

915 The Compact Muon Solenoid (CMS) is a general purpose detector designed to conduct
916 research in a wide range of physics from standard model to new physics like extra
917 dimensions and dark matter. Located at the point 5 in the LHC layout as shown in
918 Figure 3.2, CMS is composed by several detection systems distributed in a cylindrical
919 structure where the main feature is a solenoid magnet made of superconducting cable
920 capable to generate a 3.8 T magnetic field. In total, CMS weight about 14000 tons
921 in a very compact 21.6 m long and 14.6 m diameter cylinder (include areference for
922 CMS TDR). It was built in 15 separated sections at the ground level and lowered
923 to the cavern individually to be assembled. Figure 3.4 show the layout of the CMS
924 detector (CMS TDR).

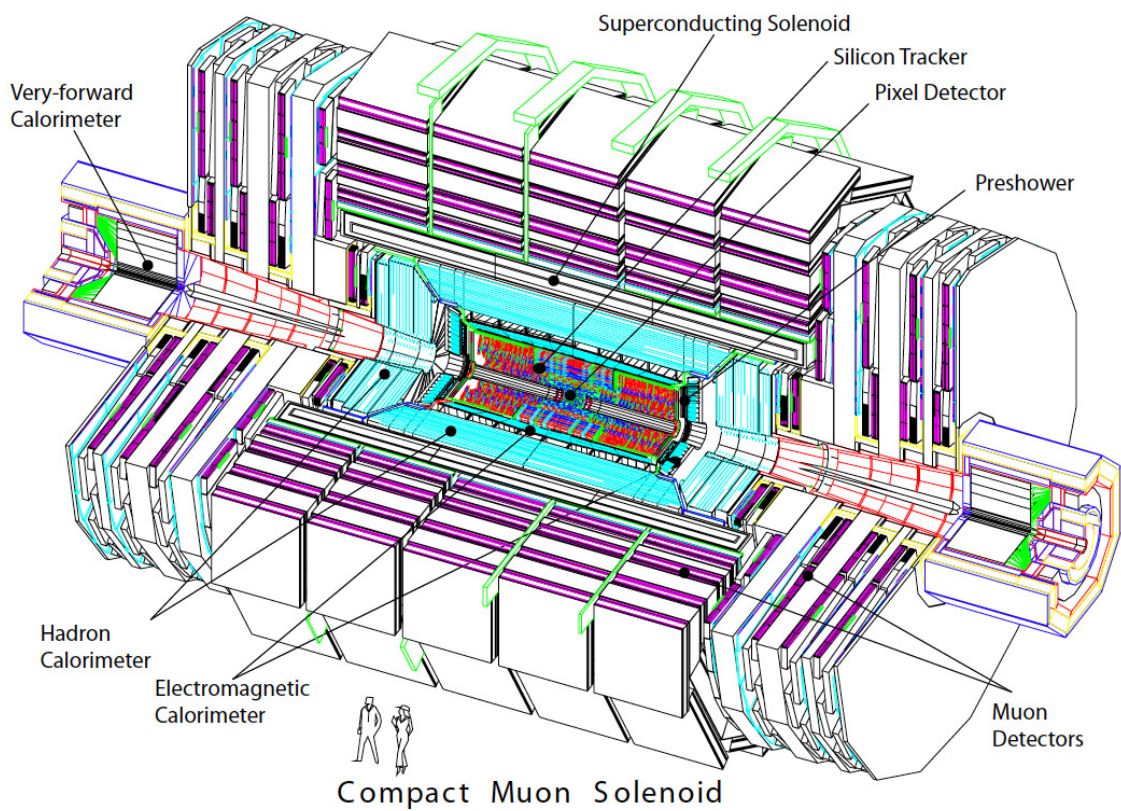


Figure 3.4: ref: CMS Collaboration, “Detector Drawings”, CMS-PHO-GEN-2012-002, <http://cds.cern.ch/record/1433717>, 2012.

925 Chapter 4

926 **Search for production of a Higgs**
927 **boson and a single top quark in**
928 **multilepton final states in pp**
929 **collisions at $\sqrt{s} = 13$ TeV**

930 4.1 Introduction

931 This chapter present the search for the associated production of a Higgs boson and
932 a single top quark events with three leptons in the final state, targeting Higgs decay
933 modes to WW , ZZ , and $\tau\tau$. The analysis uses the 13 TeV dataset produced in 2016,
934 corresponding to an integrated luminosity of 35.9fb^{-1} . It is based on and expands
935 previous analyses at 8 TeV [55, 56] and searches for associated production of $t\bar{t}$ and
936 Higgs in the same channel [57], and complements searches in other decay channels
937 targeting $H \rightarrow b\bar{b}$ [58].

938 The production cross section of the single top plus Higgs boson (tHq) process

939 is driven by a destructive interference of two main diagrams (see Fig. 4.1), where
 940 the Higgs couples to either the W boson or the top quark. Any deviation from the
 941 standard model (SM) in the Higgs coupling structure could therefore lead to a large
 942 enhancement of the cross section, making this analysis sensitive to such deviations.
 943 A second process, where the Higgs and top quark are accompanied by a W boson
 944 (tHW) has similar behavior, albeit with a weaker interference pattern.

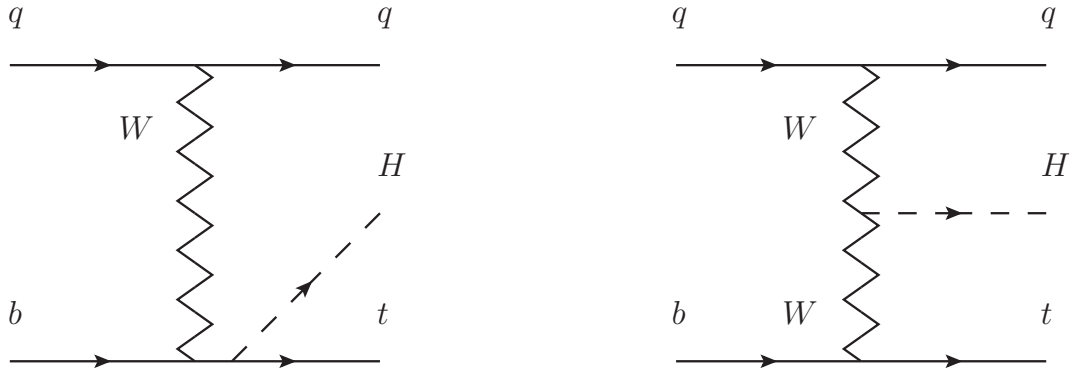


Figure 4.1: The two leading-order diagrams of tHq production.

945 We select events with three leptons and a b tagged jet in the final state. The tHq
 946 signal contribution is then determined in a fit of the observed data to two multivariate
 947 classifier outputs, each trained to discriminate against one of the two dominant back-
 948 grounds of events with non-prompt leptons from $t\bar{t}$ and of associated production of $t\bar{t}$
 949 and vector bosons ($t\bar{t}W$, $t\bar{t}Z$). The fit result is then used to set an upper limit on the
 950 combined $t\bar{t}H$, tHq and tHW production cross section, as a function of the relative
 951 coupling strengths of Higgs and top quark and Higgs and W boson, respectively.

952 4.2 Data and MC Samples

953 The data considered in this analysis were collected by the CMS experiment dur-
 954 ing 2016 and correspond to a total integrated luminosity of 35.9fb^{-1} . Only periods
 955 when the CMS magnet was on were considered when selecting the data samples, that
 956 corresponds to the 23 Sep 2016 (Run B to G) and PromptReco (Run H) versions
 957 of the datasets. The MC samples used in this analysis correspond to the RunI-
 958 ISummer16MiniAODv2 campaign produced with CMSSW 80X. The two signal sam-
 959 ples (for tHq and tHW) were produced with MG5_aMC@NLO (version 5.222), in
 960 leading-order mode, and are normalized to next-to-leading-order cross sections,
 961 see Tab. 4.1. Each sample is generated with a set of event weights corresponding to
 962 different values of κ_t and κ_V couplings as shown in Tab. 4.2.

963 4.2.1 Full 2016 dataset and MC samples

Sample	σ [pb]	BF
/THQ_Hincl_13TeV-madgraph-pythia8_TuneCUETP8M1/	0.7927	0.324
/THW_Hincl_13TeV-madgraph-pythia8_TuneCUETP8M1/	0.1472	1.0

Table 4.1: Signal samples and their cross section and branching fraction used in this analysis. See Ref. [59] for more details.

964 Different MC generators were used to generate the background processes. The
 965 dominant sources ($t\bar{t}$, $t\bar{t}W$, $t\bar{t}Z$, $t\bar{t}H$) were produced using AMC@NLO interfaced
 966 to PYTHIA8, and are scaled to NLO cross sections. Other processes are simulated
 967 using POWHEG interfaced to PYTHIA, or bare PYTHIA (see table 4.3 and [57]
 968 for more details).

		tHq			tHW		
κ_V	κ_t	sum of weights	cross section [pb]	sum of weights	cross section [pb]	LHE weights	
1.0	-3.0	35.700022	2.991	11.030445	0.6409	LHEweight_wgt[446]	
1.0	-2.0	20.124298	1.706	5.967205	0.3458	LHEweight_wgt[447]	
1.0	-1.5	14.043198	1.205	4.029093	0.2353	LHEweight_wgt[448]	
1.0	-1.25	11.429338	0.9869	3.208415	0.1876	LHEweight_wgt[449]	
1.0	-1.0		0.7927		0.1472		
1.0	-0.75	7.054998	0.6212	1.863811	0.1102	LHEweight_wgt[450]	
1.0	-0.5	5.294518	0.4723	1.339886	0.07979	LHEweight_wgt[451]	
1.0	-0.25	3.818499	0.3505	0.914880	0.05518	LHEweight_wgt[452]	
1.0	0.0	2.627360	0.2482	0.588902	0.03881	LHEweight_wgt[453]	
1.0	0.25	1.719841	0.1694	0.361621	0.02226	LHEweight_wgt[454]	
1.0	0.5	1.097202	0.1133	0.233368	0.01444	LHEweight_wgt[455]	
1.0	0.75	0.759024	0.08059	0.204034	0.01222	LHEweight_wgt[456]	
1.0	1.0	0.705305	0.07096	0.273617	0.01561	LHEweight_wgt[457]	
1.0	1.25	0.936047	0.0839	0.442119	0.02481	LHEweight_wgt[458]	
1.0	1.5	1.451249	0.1199	0.709538	0.03935	LHEweight_wgt[459]	
1.0	2.0	3.335034	0.2602	1.541132	0.08605	LHEweight_wgt[460]	
1.0	3.0	10.516125	0.8210	4.391335	0.2465	LHEweight_wgt[461]	
<hr/>							
1.5	-3.0	45.281492	3.845	13.426212	0.7825	LHEweight_wgt[462]	
1.5	-2.0	27.606715	2.371	7.809713	0.4574	LHEweight_wgt[463]	
1.5	-1.5	20.476088	1.784	5.594971	0.3290	LHEweight_wgt[464]	
1.5	-1.25	17.337465	1.518	4.635978	0.2749	LHEweight_wgt[465]	
1.5	-1.0	14.483302	1.287	3.775902	0.2244	LHEweight_wgt[466]	
1.5	-0.75	11.913599	1.067	3.014744	0.1799	LHEweight_wgt[467]	
1.5	-0.5	9.628357	0.874	2.352505	0.1410	LHEweight_wgt[468]	
1.5	-0.25	7.627574	0.702	1.789184	0.1081	LHEweight_wgt[469]	
1.5	0.0	5.911882	0.5577	1.324946	0.08056	LHEweight_wgt[470]	
1.5	0.25	4.479390	0.4365	0.959295	0.05893	LHEweight_wgt[471]	
1.5	0.5	3.331988	0.3343	0.692727	0.04277	LHEweight_wgt[472]	
1.5	0.75	2.469046	0.2558	0.525078	0.03263	LHEweight_wgt[473]	
1.5	1.0	1.890565	0.2003	0.456347	0.02768	LHEweight_wgt[474]	
1.5	1.25	1.596544	0.1689	0.486534	0.02864	LHEweight_wgt[475]	
1.5	1.5	1.586983	0.1594	0.615638	0.03509	LHEweight_wgt[476]	
1.5	2.0	2.421241	0.2105	1.170602	0.06515	LHEweight_wgt[477]	
1.5	3.0	7.503280	0.5889	3.467546	0.1930	LHEweight_wgt[478]	
<hr/>							
0.5	-3.0	27.432685	2.260	8.929074	0.5136	LHEweight_wgt[479]	
0.5	-2.0	13.956013	1.160	4.419093	0.2547	LHEweight_wgt[480]	
0.5	-1.5	8.924438	0.7478	2.757611	0.1591	LHEweight_wgt[481]	
0.5	-1.25	6.835341	0.5726	2.075247	0.1204	LHEweight_wgt[482]	
0.5	-1.0	5.030704	0.4273	1.491801	0.08696	LHEweight_wgt[483]	
0.5	-0.75	3.510528	0.2999	1.007273	0.05885	LHEweight_wgt[484]	
0.5	-0.5	2.274811	0.1982	0.621663	0.03658	LHEweight_wgt[485]	
0.5	-0.25	1.323555	0.1189	0.334972	0.01996	LHEweight_wgt[486]	
0.5	0.0	0.656969	0.06223	0.147253	0.008986	LHEweight_wgt[487]	
0.5	0.25	0.274423	0.02830	0.058342	0.003608	LHEweight_wgt[488]	
0.5	0.5	0.176548	0.01778	0.068404	0.003902	LHEweight_wgt[489]	
0.5	0.75	0.363132	0.03008	0.177385	0.009854	LHEweight_wgt[490]	
0.5	1.0	0.834177	0.06550	0.385283	0.02145	LHEweight_wgt[491]	
0.5	1.25	1.589682	0.1241	0.692099	0.03848	LHEweight_wgt[492]	
0.5	1.5	2.629647	0.2047	1.097834	0.06136	LHEweight_wgt[493]	
0.5	2.0	5.562958	0.4358	2.206057	0.1246	LHEweight_wgt[494]	
0.5	3.0	14.843102	1.177	5.609519	0.3172	LHEweight_wgt[495]	

Table 4.2: κ_V and κ_t combinations generated for the two signal samples and their NLO cross sections. The tHq cross section is multiplied by the branching fraction of the enforced leptonic decay of the top quark (0.324). See also Ref. [59].

Sample	σ [pb]
TTWJetsToLNu_TuneCUETP8M1_13TeV-amcatnloFXFX-madspin-pythia8	0.2043
TTZToLLNuNu_M-10_TuneCUETP8M1_13TeV-amcatnlo-pythia8	0.2529
ttHJetToNonbb_M125_13TeV_amcatnloFXFX_madspin_pythia8_mWCutfix /store/cmst3/group/susy/gpetrucc/13TeV/u/TTLL_m1to10_LO_NoMS_for76X/	0.2151 0.0283
WGToLNuG_TuneCUETP8M1_13TeV-madgraphMLM-pythia8	585.8
ZGTo2LG_TuneCUETP8M1_13TeV-amcatnloFXFX-pythia8	131.3
TGJets_TuneCUETP8M1_13TeV_amcatnlo_madspin_pythia8	2.967
TGJets_TuneCUETP8M1_13TeV_amcatnlo_madspin_pythia8	2.967
TTGJets_TuneCUETP8M1_13TeV-amcatnloFXFX-madspin-pythia8	3.697
WpWpJJ_EWK-QCD_TuneCUETP8M1_13TeV-madgraph-pythia8	0.03711
ZZZ_TuneCUETP8M1_13TeV-amcatnlo-pythia8	0.01398
WWZ_TuneCUETP8M1_13TeV-amcatnlo-pythia8	0.1651
WZZ_TuneCUETP8M1_13TeV-amcatnlo-pythia8	0.05565
WW_DoubleScattering_13TeV-pythia8	1.64
tZq_ll_4f_13TeV-amcatnlo-pythia8_TuneCUETP8M1	0.0758
ST_tWll_5f_LO_13TeV-MadGraph-pythia8	0.01123
TTTT_TuneCUETP8M1_13TeV-amcatnlo-pythia8	0.009103
WZTo3LNu_TuneCUETP8M1_13TeV-powheg-pythia8	4.4296
ZZTo4L_13TeV_powheg_pythia8	1.256
TTJets_SingleLeptFromTbar_TuneCUETP8M1_13TeV-madgraphMLM-pythia8	182.1754
TTJets_SingleLeptFromT_TuneCUETP8M1_13TeV-madgraphMLM-pythia8	182.1754
TTJets_DiLept_TuneCUETP8M1_13TeV-madgraphMLM-pythia8	87.3
DYJetsToLL_M-10to50_TuneCUETP8M1_13TeV-amcatnloFXFX-pythia8	18610
DYJetsToLL_M-50_TuneCUETP8M1_13TeV-madgraphMLM-pythia8	6024
WJetsToLNu_TuneCUETP8M1_13TeV-amcatnloFXFX-pythia8	61526.7
ST_tW_top_5f_inclusiveDecays_13TeV-powheg-pythia8_TuneCUETP8M1	35.6
ST_tW_antitop_5f_inclusiveDecays_13TeV-powheg-pythia8_TuneCUETP8M1	35.6
ST_t-channel_4f_leptonDecays_13TeV-amcatnlo-pythia8_TuneCUETP8M1	70.3144
ST_t-channel_antitop_4f_leptonDecays_13TeV-powheg-pythia8_TuneCUETP8M1	26.2278
ST_s-channel_4f_leptonDecays_13TeV-amcatnlo-pythia8_TuneCUETP8M1	3.68064
WWTo2L2Nu_13TeV-powheg	10.481

Table 4.3: List of background samples used in this analysis (CMSSW 80X). In the first section of the table are listed the samples of the processes for which we use the simulation to extract the final yields and shapes, in the second section the samples of the processes we will estimate from data. The MC simulation is used to design the data driven methods and derive the associated systematics.

Sample	σ [pb]
ttWJets_13TeV_madgraphMLM	0.6105
ttZJets_13TeV_madgraphMLM	0.5297/0.692

Table 4.4: Leading-order $t\bar{t}W$ and $t\bar{t}Z$ samples used in the signal BDT training.

Three lepton and Four lepton
HLT_DiMu9_Ele9_CaloIdL_TrackIdL_v*
HLT_Mu8_DiEle12_CaloIdL_TrackIdL_v*
HLT_TripleMu_12_10_5_v*
HLT_Ele16_Ele12_Ele8_CaloIdL_TrackIdL_v*
HLT_Mu23_TrkIsoVVL_Ele8_CaloIdL_TrackIdL_IsoVL_v*
HLT_Mu23_TrkIsoVVL_Ele8_CaloIdL_TrackIdL_IsoVL_DZ_v*
HLT_Mu8_TrkIsoVVL_Ele23_CaloIdL_TrackIdL_IsoVL_v*
HLT_Mu8_TrkIsoVVL_Ele23_CaloIdL_TrackIdL_IsoVL_DZ_v*
HLT_Ele23_Ele12_CaloIdL_TrackIdL_IsoVL_DZ_v*
HLT_Mu17_TrkIsoVVL_Mu8_TrkIsoVVL_DZ_v*
HLT_Mu17_TrkIsoVVL_TkMu8_TrkIsoVVL_DZ_v*
HLT_IsoMu22_v*
HLT_IsoTkMu22_v*
HLT_IsoMu22_eta2p1_v*
HLT_IsoTkMu22_eta2p1_v*
HLT_IsoMu24_v*
HLT_IsoTkMu24_v*
HLT_Ele27_WPTight_Gsf_v*
HLT_Ele25_eta2p1_WPTight_Gsf_v*
HLT_Ele27_eta2p1_WPLoose_Gsf_v*

Table 4.5: Table of high-level triggers that we consider in the analysis.

969 4.2.2 Triggers

970 We consider online-reconstructed events triggered by one, two, or three leptons.
 971 Single-lepton triggers are included to boost the acceptance of events where the p_T of
 972 the sub-leading lepton falls below the threshold of the double-lepton triggers. Ad-
 973 ditionally, by including double-lepton triggers in the ≥ 3 lepton category, as well
 974 as single-lepton triggers in all categories, we increase the efficiency, considering the
 975 logical “or” of the trigger decisions of all the individual triggers in a given category.
 976 Tab. 4.5 shows the lowest-threshold non-prescaled triggers present in the High-Level
 977 Trigger (HLT) menus for both Monte-Carlo and data in 2016.

978 4.2.2.1 Trigger efficiency scale factors

979 The efficiency of events to pass the trigger is measured in simulation (trivially using
 980 generator information) and in the data (using event collected by an uncorrelated

Category	Scale Factor
ee	1.01 ± 0.02
e μ	1.01 ± 0.01
$\mu\mu$	1.00 ± 0.01
3l	1.00 ± 0.03

Table 4.6: Trigger efficiency scale factors and associated uncertainties, shown here rounded to the nearest percent.

981 MET trigger). Small differences between the data and MC efficiencies are corrected
 982 by applying scale factors as shown in Tab. 4.6. The exact procedure and control plots
 983 are documented in [60] for the current analysis.

984 4.3 Object Identification and event selection

985 4.3.1 Jets and b tagging

986 The analysis uses anti- k_t (0.4) particle-flow (PF) jets, corrected for charged hadrons
 987 not coming from the primary vertex (charged hadron subtraction), and having jet
 988 energy corrections (`Summer16_23Sep2016V3`) applied as a function of the jet E_T and
 989 η . Jets are only considered if they have a transverse energy above 25GeV.

990 In addition, they are required to be separated from any lepton candidates passing
 991 the fakeable object selections (see Tables 4.7 and 4.8) by $\Delta R > 0.4$.

992 The loose and medium working points of the CSV b-tagging algorithm are used to
 993 identify b jets. Data/simulation differences in the b tagging performance are corrected
 994 by applying per-jet weights to the simulation, dependent on the jet p_T , eta, b tagging
 995 discriminator, and flavor (from simulation truth) [61]. The per-event weight is taken
 996 as the product of the per-jet weights, including those of the jets associated to the
 997 leptons. More details can be found in the corresponding $t\bar{t}H$ documentation [57, 60].

998 **4.3.2 Lepton selection**

Cut	Loose	Fakeable object	Tight
$ \eta < 2.4$	✓	✓	✓
p_T	$> 5\text{GeV}$	$> 15\text{GeV}$	$> 15\text{GeV}$
$ d_{xy} < 0.05 \text{ (cm)}$	✓	✓	✓
$ d_z < 0.1 \text{ (cm)}$	✓	✓	✓
$\text{SIP}_{3D} < 8$	✓	✓	✓
$I_{\text{mini}} < 0.4$	✓	✓	✓
is Loose Muon	✓	✓	✓
jet CSV	—	< 0.8484	< 0.8484
is Medium Muon	—	—	✓
tight-charge	—	—	✓
lepMVA > 0.90	—	—	✓

Table 4.7: Requirements on each of the three muon selections. In the cases where the cut values change between the selections, those values are listed in the table. Otherwise, whether the cut is applied is indicated. For the two p_T^{ratio} and CSV rows, the cuts marked with a † are applied to leptons that fail the lepton MVA cut, while the loose cut value is applied to those that pass the lepton MVA cut.

999 The lepton reconstruction and selection is identical to that used in the $t\bar{t}H$ mul-
1000 tilepton analysis, as documented in Refs. [57, 60]. For details on the reconstruction
1001 algorithms, isolation, pileup mitigation, and a description of the lepton MVA discrim-
1002 inator and validation plots thereof, we refer to that document since they are out of
1003 the scope of this thesis. Three different selections are defined both for the electron
1004 and muon object identification: the *Loose*, *Fakeable Object*, and *Tight* selection. As
1005 described in more detail later, these are used for event level vetoes, the fake rate
1006 estimation application region, and the final signal selection, respectively. The p_T of
1007 fakeable objects is defined as $0.85 \times p_T(\text{jet})$, where the jet is the one associated to the
1008 lepton object. This mitigates the dependence of the fake rate on the momentum of
1009 the fakeable object and thereby improves the precision of the method.

1010 Tables 4.7 and 4.8 list the full criteria for the different selections of muons and
1011 electrons.

Cut	Loose	Fakeable Object	Tight
$ \eta < 2.5$	✓	✓	✓
p_T	$> 7\text{GeV}$	$> 15\text{GeV}$	$> 15\text{GeV}$
$ d_{xy} < 0.05 \text{ (cm)}$	✓	✓	✓
$ d_z < 0.1 \text{ (cm)}$	✓	✓	✓
$\text{SIP}_{3D} < 8$	✓	✓	✓
$I_{\text{mini}} < 0.4$	✓	✓	✓
MVA ID $> (0.0, 0.0, 0.7)$	✓	✓	✓
$\sigma_{i\eta i\eta} < (0.011, 0.011, 0.030)$	—	✓	✓
$\text{H/E} < (0.10, 0.10, 0.07)$	—	✓	✓
$\Delta\eta_{in} < (0.01, 0.01, 0.008)$	—	✓	✓
$\Delta\phi_{in} < (0.04, 0.04, 0.07)$	—	✓	✓
$-0.05 < 1/E - 1/p < (0.010, 0.010, 0.005)$	—	✓	✓
p_T^{ratio}	—	$> 0.5 \dagger / -$	—
jet CSV	—	$< 0.3 \dagger / < 0.8484$	< 0.8484
tight-charge	—	—	✓
conversion rejection	—	—	✓
Number of missing hits	< 2	$== 0$	$== 0$
lepMVA > 0.90	—	—	✓

Table 4.8: Criteria for each of the three electron selections. In cases where the cut values change between selections, those values are listed in the table. Otherwise, whether the cut is applied is indicated. In some cases, the cut values change for different η ranges. These ranges are $0 < |\eta| < 0.8$, $0.8 < |\eta| < 1.479$, and $1.479 < |\eta| < 2.5$ and the respective cut values are given in the form (value₁, value₂, value₃).

4.3.3 Lepton selection efficiency

Efficiencies of reconstruction and selecting loose leptons are measured both for muons and electrons using a tag and probe method on both data and MC, using $Z \rightarrow \ell^+\ell^-$. Corresponding scale factors are derived from the ratio of efficiencies and applied to the selected These. Events are produced for the leptonic SUSY analyses using equivalent lepton selections and recycled for the $t\bar{t}H$ analysis as well as for this analysis. The efficiencies of applying the tight selection as defined in Tables 4.7 and 4.8, on the loose leptons are determined again by using a tag and probe method on a sample of DY-enriched events. They are documented for the $t\bar{t}H$ analysis in Ref. [60] and are exactly equivalent for this analysis.

1022 4.4 Background predictions

1023 The modeling of reducible and irreducible backgrounds in this analysis uses the exact
 1024 methods, analysis code, and ROOT trees used for the $t\bar{t}H$ multilepton analysis. We
 1025 give a brief description of the methods and refer to the documentation of that analysis
 1026 in Refs. [57, 60] for any details.

1027 The backgrounds in three-lepton final states can be split in two broad categories:
 1028 irreducible backgrounds with genuine prompt leptons (i.e. from on-shell W and Z
 1029 boson decays); and reducible backgrounds where at least one of the leptons is “non-
 1030 prompt”, i.e. produced within a hadronic jet, either a genuine lepton from heavy
 1031 flavor decays, or simply mis-reconstructed jets.

1032 Irreducible backgrounds can be reliably estimated directly from Monte-Carlo sim-
 1033 ulated events, using higher-order cross sections or data control regions for the overall
 1034 normalization. This is done in this analysis for all backgrounds involving prompt lep-
 1035 tons: $t\bar{t}W$, $t\bar{t}Z$, $t\bar{t}H$, WZ , ZZ , $W^\pm W^\pm qq$, $t\bar{t}t\bar{t}$, tZq , tZW , WWW , WWZ , WZZ ,
 1036 ZZZ .

1037 Reducible backgrounds, on the other hand, are not well predicted by simulation,
 1038 and are estimated using data-driven methods. In the case of non-prompt leptons, a
 1039 fake rate method is used, where the contribution to the final selection is estimated by
 1040 extrapolating from a sideband (or “application region”) with a looser lepton definition
 1041 (the fakeable object definitions in Tabs. 4.7 and 4.8) to the signal selection. The tight-
 1042 to-loose ratios (or “fake rates”) are measured in several background dominated data
 1043 events with dedicated triggers, subtracting the residual prompt lepton contribution
 1044 using MC. Non-prompt leptons in our signal regions are predominantly produced in $t\bar{t}$
 1045 events, with a much smaller contribution, from Drell–Yan production. The systematic
 1046 uncertainty on the normalization of the non-prompt background estimation is on the

order of 50%, and thereby one of the dominant limitations on the performance of multilepton analyses in general and this analysis in particular. It consists of several individual sources, such as the result of closure tests of the method using simulated events, limited statistics in the data control regions due to necessary prescaling of lepton triggers, and the uncertainty in the subtraction of residual prompt leptons from the control region.

The fake background where the leptons pass the looser selection are weighted according to how many of them fail the tight criteria. Events with a single failing lepton are weighted with the factor $f/(1-f)$ for the estimate to the tight selection region, where f is the fake rate. Events with two failing leptons are given the negative weight $-f_i f_j / (1-f_i)(1-f_j)$, and for three leptons the weight is positive and equal to the product of $f/(1-f)$ factor evaluated for each failing lepton.

Figures 4.2 show the distributions of some relevant kinematic variables, normalized to the cross section of the respective processes and to the integrated luminosity.

4.5 Signal discrimination

The tHq signal is separated from the main backgrounds using a boosted decision tree (BDT) classifier, trained on simulated signal and background events. A set of discriminating variables are given as input to the BDT which produces a output distribution maximizing the discrimination power. Table 4.9 lists the input variables used while Figures 4.3 show their distributions for the relevant signal and background samples, for the three lepton channel. Two BDT classifiers are trained for the two main backgrounds expected in the analysis: events with prompt leptons from $t\bar{t}W$ and $t\bar{t}Z$ (also referred to as $t\bar{t}V$), and events with non-prompt leptons from $t\bar{t}$. The datasets used in the training are the tHq signal (see Tab. 4.1), and LO MADGRAPH samples

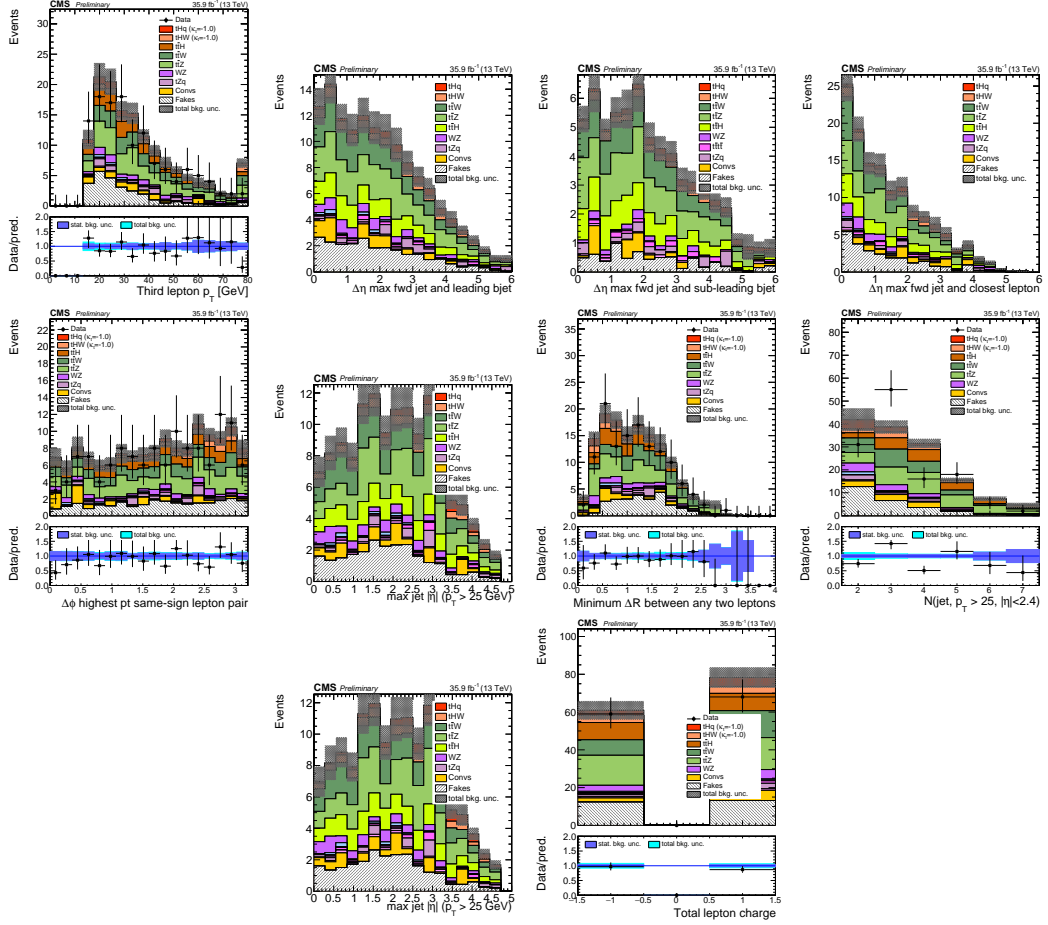


Figure 4.2: Distributions of input variables to the BDT for signal discrimination, three lepton channel, normalized to their cross section and to 35.9fb^{-1} .

of $t\bar{t}W$ and $t\bar{t}Z$, in an admixture proportional to their respective cross sections (see Tab. 4.4).

The MVA analysis consist of two stages: first a “training” where the MVA method is trained to discriminate between simulated signal and background events, then a “test” stage where the trained algorithm is used to classify different events from the samples. The sample is obtained from a pre-selection (see Tab. ?? with pre-selection cuts). Figures 4.4 show the input variables distributions as seen by the MVA algorithm. Note that in contrast to the distributions in Fig. 4.3 only the main backgrounds ($t\bar{t}$ from simulation, $t\bar{t}V$) are included.

Variable name	Description
nJet25	Number of jets with $p_T > 25$ GeV, $ \eta < 2.4$
MaxEtaJet25	Maximum $ \eta $ of any (non-CSV-loose) jet with $p_T > 25$ GeV
totCharge	Sum of lepton charges
nJetEta1	Number of jets with $ \eta > 1.0$, non-CSV-loose
detaFwdJetBJet	$\Delta\eta$ between forward light jet and hardest CSV loose jet
detaFwdJet2BJet	$\Delta\eta$ between forward light jet and second hardest CSV loose jet (defaults to -1 in events with only one CSV loose jet)
detaFwdJetClosestLep	$\Delta\eta$ between forward light jet and closest lepton
dphiHighestPtSSPair	$\Delta\phi$ of highest p_T same-sign lepton pair
minDRll	minimum ΔR between any two leptons
Lep3Pt/Lep2Pt	p_T of the 3 rd lepton (2 nd for ss2l)

Table 4.9: MVA input discriminating variables

1080 Note that splitting the training in two groups reveals that some variables show
 1081 opposite behavior for the two background sources; potentially screening the discrimi-
 1082 nation power if they were to be used in a single discriminant. For some other variables
 1083 the distributions are similar in both background cases.

1084 From table 4.9, it is clear that the input variables are correlated to some extend.
 1085 These correlations play an important role for some MVA methods like the Fisher
 1086 discriminant method in which the first step consist of performing a linear transfor-
 1087 mation to an phase space where the correlations between variables are removed. In
 1088 case a boosted decision tree (BDT) method however, correlations do not affect the
 1089 performance. Figure 4.6 show the linear correlation coefficients for signal and back-
 1090 ground for the two training cases (the signal values are identical by construction). As
 1091 expected, strong correlations appears for variables related to the forward jet activity.
 1092 Same trend is seen in case of the same sign dilepton channel in Figure ??.

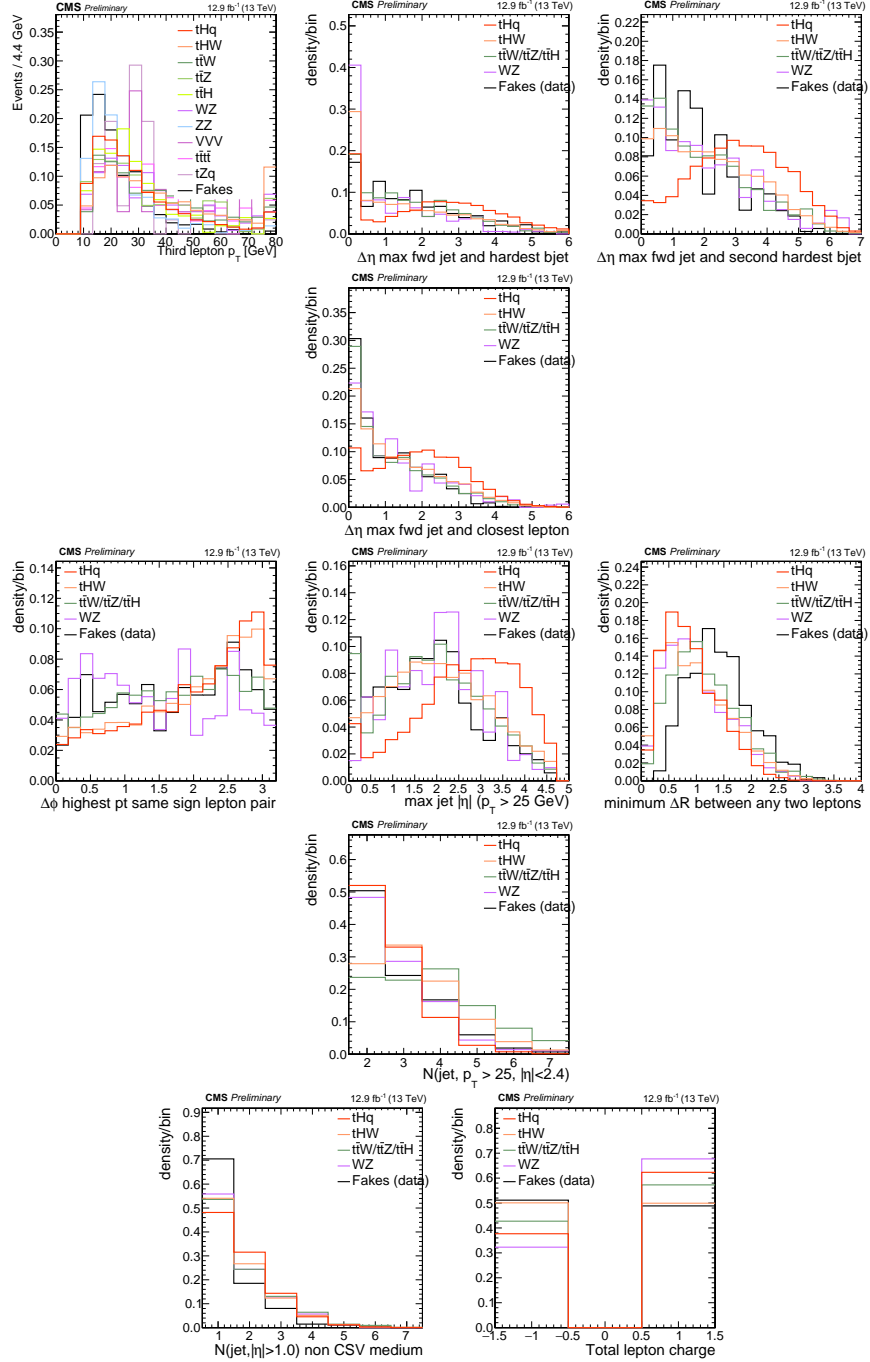


Figure 4.3: Distributions of input variables to the BDT for signal discrimination, three lepton channel.

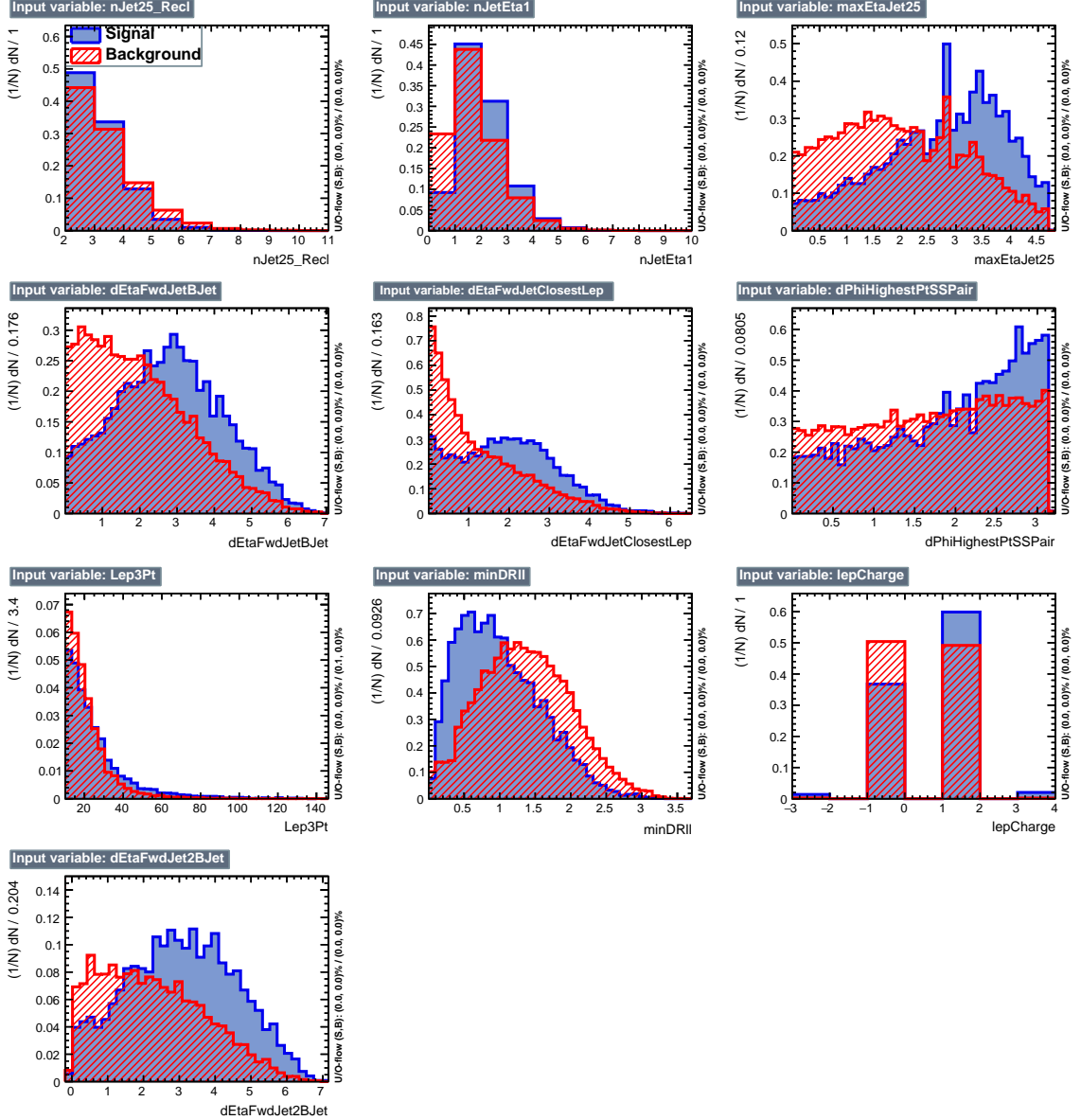


Figure 4.4: BDT inputs as seen by TMVA (signal, in blue, is tHq , background, in red, is $t\bar{t}$) for the three lepton channel, discriminated against $t\bar{t}$ (fakes) background.

1093 4.5.1 Classifiers response

1094 Several MVA algorithms were evaluated to determine the most appropriate method
 1095 for this analysis. The plots in Fig. 4.7 (top) show the background rejection as a
 1096 function of the signal efficiency for $t\bar{t}$ and $t\bar{t}V$ trainings (ROC curves) for the different

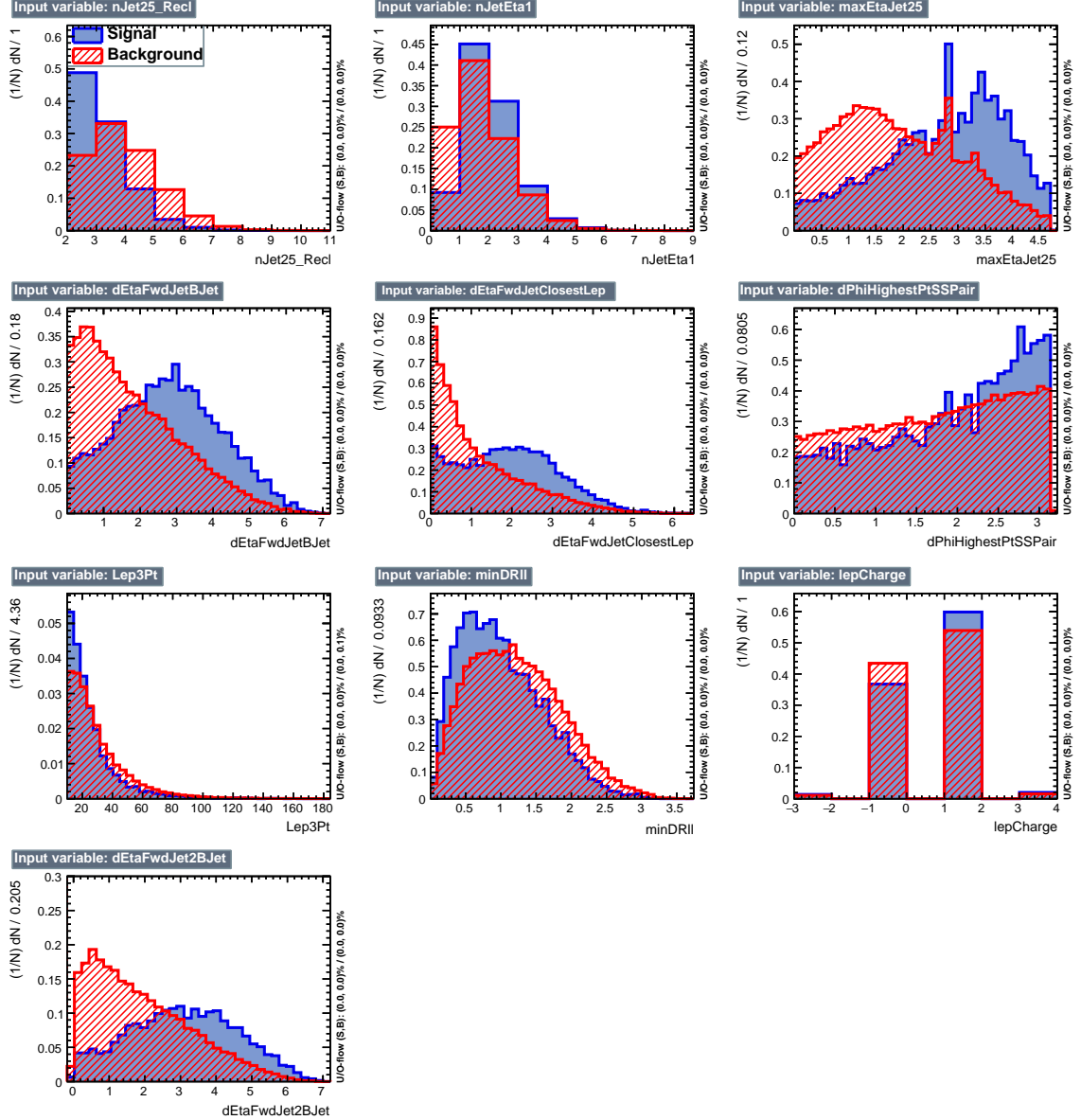


Figure 4.5: BDT inputs as seen by TMVA (signal, in blue, is tHq , background, in red, is $t\bar{t}W+t\bar{t}Z$) for the three lepton channel, discriminated against $t\bar{t}V$ background.

algorithms that were evaluated.

In both cases the gradient boosted decision tree (“BDTA_GRAD”) classifier offers the best results, followed by an adaptive BDT classifier (“BDTA”). The BDTA_GRAD classifier output distributions for signal and backgrounds are shown on the bottom of Fig. 4.7. As expected, a good discrimination power is obtained using default discrim-

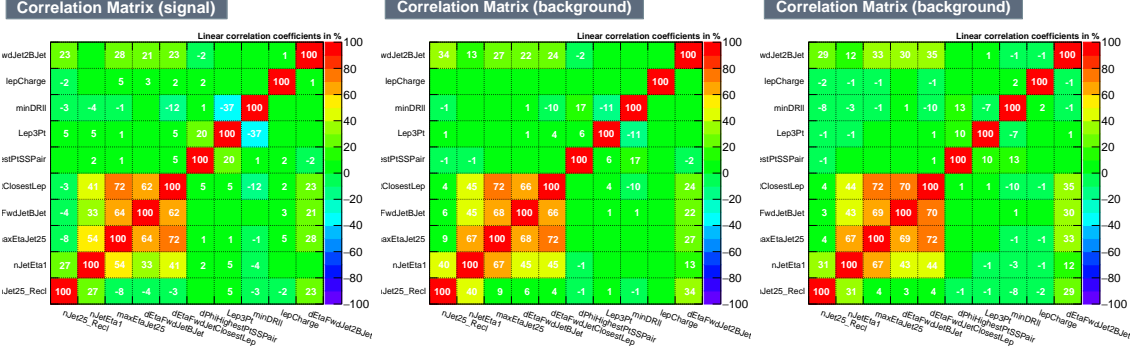


Figure 4.6: Signal (left), $t\bar{t}$ background (middle), and $t\bar{t}V$ background (right.) correlation matrices for the input variables in the TMVA analysis for the three lepton channel.

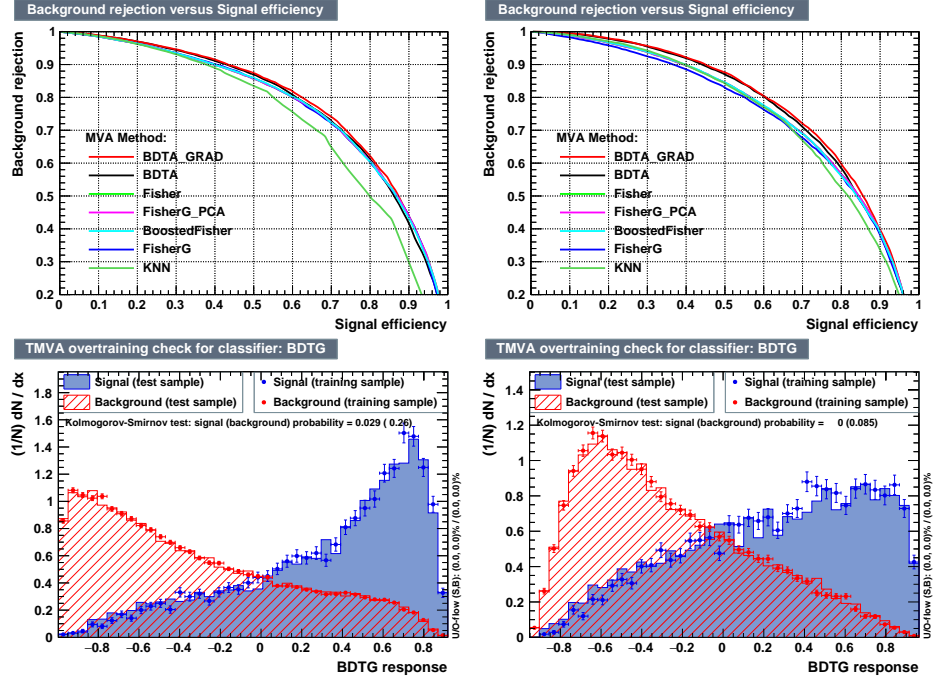


Figure 4.7: Top: background rejection vs signal efficiency (ROC curves) for various MVA classifiers (top) in the three lepton channel against $t\bar{t}V$ (left) and $t\bar{t}$ (right). Bottom: classifier output distributions for the gradient boosted decision trees, for training against $t\bar{t}V$ (left) and against $t\bar{t}$ (right).

inatory parameter values, with minimal overtraining. TMVA provides a ranking of the
input variables by their importance in the classification process, shown in Tab. 4.10.
The TMVA settings used in the BDT training are shown in Tab. 4.11.

ttbar training			ttV training		
Rank	Variable	Importance	Variable	Importance	
1	minDRll	1.329e-01	dEtaFwdJetBJet	1.264e-01	
2	dEtaFwdJetClosestLep	1.294e-01	Lep3Pt	1.224e-01	
3	dEtaFwdJetBJet	1.209e-01	maxEtaJet25	1.221e-01	
4	dPhiHighestPtSSPair	1.192e-01	dEtaFwdJet2BJet	1.204e-01	
5	Lep3Pt	1.158e-01	dEtaFwdJetClosestLep	1.177e-01	
6	maxEtaJet25	1.121e-01	minDRll	1.143e-01	
7	dEtaFwdJet2BJet	9.363e-02	dPhiHighestPtSSPair	9.777e-02	
8	nJetEta1	6.730e-02	nJet25_Recl	9.034e-02	
9	nJet25_Recl	6.178e-02	nJetEta1	4.749e-02	
10	lepCharge	4.701e-02	lepCharge	4.116e-02	

Table 4.10: TMVA input variables ranking for BDTA_GRAD method for the trainings in the three lepton channel. For both trainings the rankings show almost the same 5 variables in the first places.

```
TMVA.Types.kBDT
NTrees=800
BoostType=Grad
Shrinkage=0.10
!UseBaggedGrad
nCuts=50
MaxDepth=3
NegWeightTreatment=PairNegWeightsGlobal
CreateMVApdfs
```

Table 4.11: TMVA configuration used in the BDT training.

1105 4.6 Additional discriminating variables

1106 Two additional discriminating variables were tested considering the fact that the
 1107 forward jet in the background could come from the pileup; since we have a real
 1108 forward jet in the signal, it could give some improvement in the discriminating power.
 1109 The additional variables describe the forward jet momentum (fwdJetPt25) and the
 1110 forward jet identification(fwdJetPUID). Distributions for these variables in the three
 1111 lepton channel are shown in the figure 4.8. The forward jet identification distribution
 1112 show that for both, signal and background, jets are mostly real jets.

1113 The testing was made including in the MVA input one variable at a time, so we

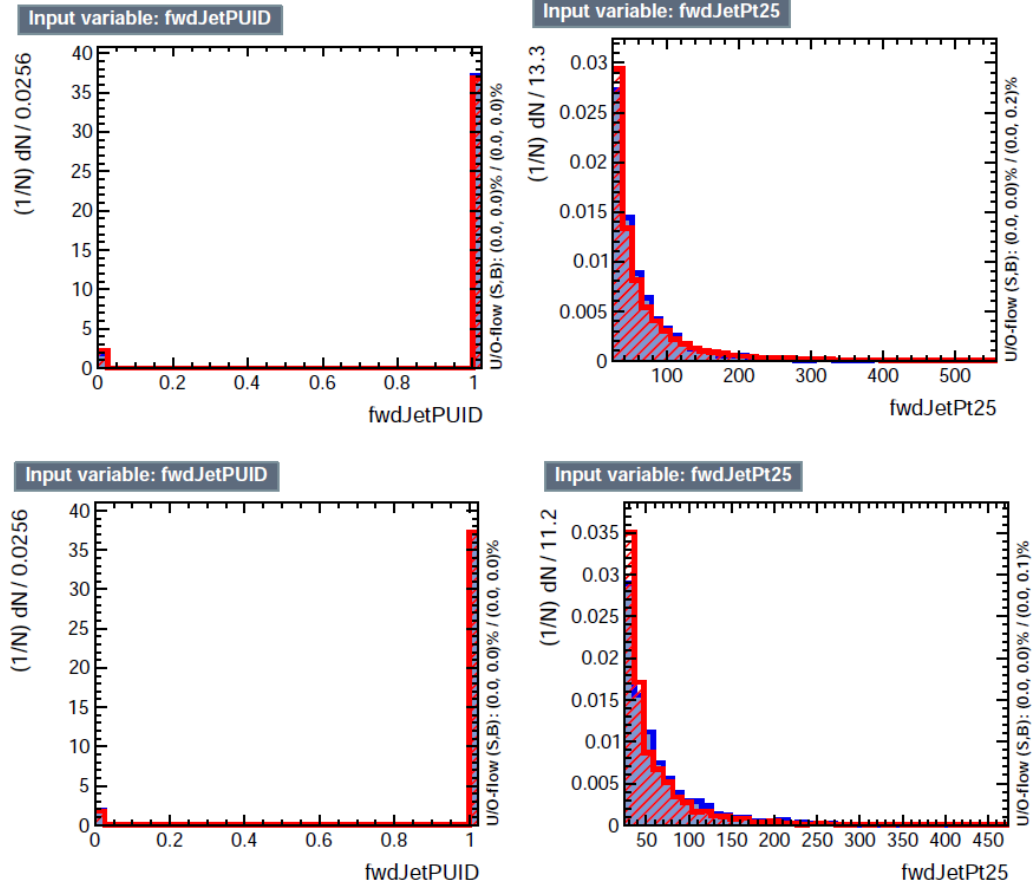


Figure 4.8: Additional discriminating variables distributions for ttV training (Top row) and tt training (bottom row) in the three lepton channel. The origin of the jets in the forward jet identification distribution is tagged as 0 for “pileup jets” while “real jets” are tagged as 1.

1114 can evaluate the discrimination power of each variable, and then both simultaneously.
 1115 fwdJetPUID was ranked in the last place in importance (11) in both training (ttV
 1116 and tt) while fwdJetPt25 was ranked 3 in the ttV training and 7 in the tt training.
 1117 When training using 12 variables, fwdJetPt25 was ranked 5 and 7 in the ttV and tt
 1118 trainings respectively, while fwdJetPUID was ranked 12 in both cases.

1119 The improvement in the discrimination performance provided by the additional
 1120 variables is about 1%, so it was decided not to include them in the procedure. Table
 1121 4.12 show the ROC-integral for all the testing cases we made.

ROC-integral	
base 10 var ttv	0.848
+ fwdJetPUID ttv	0.849
+ fwdJetPt25 ttv	0.856
12 var ttv	0.856
<hr/>	
base 10 var tt	0.777
+ fwdJetPUID tt	0.777
+ fwdJetPt25 tt	0.787
12 var	0.787

Table 4.12: ROC-integral for all the testing cases we made in the evaluation of the additional variables discriminating power. The improvement in the discrimination performance provided by the additional variables is about 1%

₁₁₂₂ **Chapter 5**

₁₁₂₃ **The CMS forward pixel detector**

₁₁₂₄ **5.0.1 The phase 1 FPix upgrade**

₁₁₂₅ **5.0.2 FPix module production line**

₁₁₂₆ **5.0.3 The Gluing stage**

₁₁₂₇ **5.0.4 The Encapsulation stage**

₁₁₂₈ **5.0.5 The FPix module production yields**

1129 References

- 1130 [1] D.J. Griffiths, “Introduction to electrodynamics”. 4th ed. Pearson, (2013).
- 1131 [2] F. Mandl, G. Shaw. “Quantum field theory.” Chichester: Wiley (2009).
- 1132 [3] F. Halzen, and A.D. Martin, “Quarks and leptons: An introductory course in
1133 modern particle physics”. New York: Wiley, (1984) .
- 1134 [4] J.C. Maxwell. “A dynamical theory of the electromagnetic field”. Philosophical
1135 Transactions of the Royal Society of London. 155: 459â€¢512.(1865)
1136 doi:10.1098/rstl.1865.0008
- 1137 [5] M. Planck. “ÃIJber das Gesetz der Energieverteilung im Normalspektrum”.
1138 Annalen der Physik. 4 (3): 553.(1901).
- 1139 [6] A. Einstein “ÃIJber einen die Erzeugung und Verwandlung des Lichtes betref-
1140 fenden heuristischen Gesichtspunkt”. Annalen der Physik. 17 (6): 132â€¢148,
1141 (1905).
- 1142 [7] A. Einstein. “ÃIJber die von der molekularkinetischen Theorie der WÃdrme
1143 geforderte Bewegung von in ruhenden FlÃijssigkeiten suspendierten Teilchen”.
1144 Annalen der Physik. 17 (8): 549â€¢560, (1905).
- 1145 [8] A. Einstein. “Zur Elektrodynamik bewegter KÃürper”. Annalen der Physik. 17
1146 (10): 891â€¢921, (1905).

- 1147 [9] A. Einstein, "Ist die TrÄdgheit eines KÃürpers von seinem Energieinhalt ab-
 1148 hÃdngig?". Annalen der Physik. 18 (13): 639â€¢641, (1905).
- 1149 [10] B. P. Abbott et al. "Observation of Gravitational Waves from a Binary Black
 1150 Hole Merger". PRL 116, 061102 (2016).
- 1151 [11] J. Schwinger. "Quantum Electrodynamics. I. A Covariant Formulation". Phys-
 1152 ical Review. 74 (10): 1439â€¢61, (1948).
- 1153 [12] R. P. Feynman. "Spaceâ€¢Time Approach to Quantum Electrodynamics".
 1154 Physical Review. 76 (6): 769â€¢89, (1949).
- 1155 [13] S. Tomonaga. "On a Relativistically Invariant Formulation of the Quantum
 1156 Theory of Wave Fields". Progress of Theoretical Physics. 1 (2): 27â€¢42, (1946).
- 1157 [14] S.L. Glashow. "Partial symmetries of weak interactions", Nucl. Phys. 22 579-
 1158 588, (1961).
- 1159 [15] A. Salam, J.C. Ward. "Electromagnetic and weak interactions", Physics Letters
 1160 13 168-171, (1964).
- 1161 [16] S. Weinberg, "A model of leptons", Physical Review Letters, vol. 19, no. 21, p.
 1162 1264, (1967).
- 1163 [17] E. Noether, "Invariante Variationsprobleme", Nachrichten von der Gesellschaft
 1164 der Wissenschaften zu GÃüttingen, mathematisch-physikalische Klasse, vol.
 1165 1918, pp. 235â€¢257, (1918).
- 1166 [18] File:Standard_Model_of_Elementary_Particle_dark.svg. (2017, June 12)
 1167 Wikimedia Commons, the free media repository. Retrieved November 27,
 1168 2017 from <https://www.collegiate-advanced-electricity.com/single-post/2017/04/10/The-Standard-Model-of-Particle-Physics>.

- 1170 [19] M. Goldhaber, L. Grodzins, A.W. Sunyar “Helicity of Neutrinos”, Phys. Rev.
 1171 109, 1015 (1958).
- 1172 [20] Palanque-Delabrouille N et al. “Neutrino masses and cosmology with Lyman-
 1173 alpha forest power spectrum”, JCAP 11 011 (2015).
- 1174 [21] C. Patrignani et al. (Particle Data Group), Chin. Phys. C, 40, 100001 (2016)
 1175 and 2017 update.
- 1176 [22] M. Gell-Mann. “A Schematic Model of Baryons and Mesons”. Physics Letters.
 1177 8 (3): 214–215 (1964).
- 1178 [23] G. Zweig. “An SU(3) Model for Strong Interaction Symmetry and its Breaking”
 1179 (PDF). CERN Report No.8182/TH.401 (1964).
- 1180 [24] G. Zweig. “An SU(3) Model for Strong Interaction Symmetry and its Breaking:
 1181 II” (PDF). CERN Report No.8419/TH.412(1964).
- 1182 [25] M. Gell-Mann. “The Interpretation of the New Particles as Displaced Charged
 1183 Multiplets”. Il Nuovo Cimento 4: 848. (1956).
- 1184 [26] T. Nakano, K. Nishijima. “Charge Independence for V-particles”. Progress of
 1185 Theoretical Physics 10 (5): 581-582. (1953).
- 1186 [27] N. Cabibbo, “Unitary symmetry and leptonic decays” Physical Review Letters,
 1187 vol. 10, no. 12, p. 531, (1963).
- 1188 [28] M.Kobayashi, T.Maskawa, “CP-violation in the renormalizable theory of weak
 1189 interaction,” Progress of Theoretical Physics, vol. 49, no. 2, pp. 652-657, (1973).
- 1190 [29] File:Weak Decay (flipped).svg. (2017, June 12). Wikimedia Commons, the free media repository. Retrieved November 27, 2017

- 1192 from `https : //commons.wikimedia.org/w/index.php?title = File :`
 1193 `Weak_Decay_(flipped).svg&oldid = 247498592.`
- 1194 [30] Georgia Tech University. Coupling Constants for the Fundamental
 1195 Forces(2005). Retrieved January 10, 2018, from `http://hyperphysics.phy –`
 1196 `astr.gsu.edu/hbase/Forces/couple.html#c2`
- 1197 [31] M. Strassler. (May 31, 2013).The Strengths of the Known Forces. Retrieved
 1198 January 10, 2018, from `https://profmattstrassler.com/articles – and –`
 1199 `posts/particle – physics – basics/the – known – forces – of – nature/the –`
 1200 `strength – of – the – known – forces/`
- 1201 [32] M. Peskin, D. Schroeder, “An introduction to quantum field theory”. Perseus
 1202 Books Publishing L.L.C., (1995).
- 1203 [33] A. Pich. “The Standard Model of Electroweak Interactions”
 1204 `https://arxiv.org/abs/1201.0537`
- 1205 [34] F.Bellaiche. (2012, 2 September). “What’s this Higgs boson anyway?”. Retrieved
 1206 from: `https://www.quantum-bits.org/?p=233`
- 1207 [35] M. Endres et al. Nature 487, 454-458 (2012) doi:10.1038/nature11255
- 1208 [36] F. Englert, R. Brout. “Broken Symmetry and the Mass of Gauge Vec-
 1209 tor Mesons”. Physical Review Letters. 13 (9): 321–323.(1964) Bib-
 1210 code:1964PhRvL..13..321E. doi:10.1103/PhysRevLett.13.321
- 1211 [37] P.Higgs. “Broken Symmetries and the Masses of Gauge Bosons”. Physical
 1212 Review Letters. 13 (16): 508–509,(1964). Bibcode:1964PhRvL..13..508H.
 1213 doi:10.1103/PhysRevLett.13.508.

- 1214 [38] G.Guralnik, C.R. Hagen and T.W.B. Kibble. “Global Conservation Laws and
 1215 Massless Particles”. Physical Review Letters. 13 (20): 585–587, (1964). Bib-
 1216 code:1964PhRvL..13..585G. doi:10.1103/PhysRevLett.13.585.
- 1217 [39] CMS collaboration. “Observation of a new boson at a mass of 125
 1218 GeV with the CMS experiment at the LHC”. Physics Letters B.
 1219 716 (1): 30–61 (2012). arXiv:1207.7235. Bibcode:2012PhLB..716...30C.
 1220 doi:10.1016/j.physletb.2012.08.021
- 1221 [40] ATLAS collaboration. “Observation of a New Particle in the Search for the Stan-
 1222 dard Model Higgs Boson with the ATLAS Detector at the LHC”. Physics Let-
 1223 ters B. 716 (1): 1–29(2012). arXiv:1207.7214 Bibcode:2012PhLB..716....1A.
 1224 doi:10.1016/j.physletb.2012.08.020.
- 1225 [41] ATLAS collaboration; CMS collaboration (26 March 2015). “Combined
 1226 Measurement of the Higgs Boson Mass in pp Collisions at $\sqrt{s}=7$ and
 1227 8 TeV with the ATLAS and CMS Experiments”. Physical Review Let-
 1228 ters. 114 (19): 191803. arXiv:1503.07589. Bibcode:2015PhRvL.114s1803A.
 1229 doi:10.1103/PhysRevLett.114.191803.
- 1230 [42] CMS Collaboration, “SM Higgs Branching Ratios and To-
 1231 tal Decay Widths (up-date in CERN Report4 2016)”.
 1232 <https://twiki.cern.ch/twiki/bin/view/LHCPhysics/CERNYellowReportPageBR>
 1233 , last accessed on 17.12.2017.
- 1234 [43] R.Grant V. “Determination of Higgs branching ratios in $H \rightarrow W^+W^- \rightarrow l^+l^- jj$ and $H \rightarrow ZZ \rightarrow l^+l^- jj$ channels”. Physics Department, Uni-
 1235 versity of Tennessee (Dated: October 31, 2012). Retrieved from
 1236 <http://aesop.phys.utk.edu/ph611/2012/projects/Riley.pdf>

- 1238 [44] LHC Higgs Cross Section Working Group, Denner, A., Heinemeyer, S. et al.
 1239 “Standard model Higgs-boson branching ratios with uncertainties”. Eur. Phys.
 1240 J. C (2011) 71: 1753. <https://doi.org/10.1140/epjc/s10052-011-1753-8>
- 1241 [45] LHC InternationalMasterclasses“When protons collide”. Retrieved from
 1242 http://atlas.physicsmasterclasses.org/en/zpath_protoncollisions.htm
- 1243 [46] F. Maltoni, K. Paul, T. Stelzer, and S. Willenbrock, “Associated production
 1244 of Higgs and single top at hadron colliders”, Phys.Rev. D64 (2001) 094023,
 1245 [hep-ph/0106293].
- 1246 [47] S. Biswas, E. Gabrielli, F. Margaroli, and B. Mele, “Direct constraints on the
 1247 top-Higgs coupling from the 8 TeV LHC data,” Journal of High Energy Physics,
 1248 vol. 07, p. 073, (2013).
- 1249 [48] M. Farina, C. Grojean, F. Maltoni, E. Salvioni, and A. Thamm, “Lifting de-
 1250 generacies in Higgs couplings using single top production in association with a
 1251 Higgs boson,” Journal of High Energy Physics, vol. 05, p. 022, (2013).
- 1252 [49] T.M. Tait and C.-P. Yuan, “Single top quark production as a window to physics
 1253 beyond the standard model”, Phys. Rev. D 63 (2000) 014018 [hep-ph/0007298].
- 1254 [50] F. Demartin, F. Maltoni, K. Mawatari, and M. Zaro, “Higgs production in
 1255 association with a single top quark at the LHC,” European Physical Journal C,
 1256 vol. 75, p. 267, (2015).
- 1257 [51] CMS Collaboration, “Modelling of the single top-quark pro-
 1258 duction in association with the Higgs boson at 13 TeV.”
 1259 <https://twiki.cern.ch/twiki/bin/viewauth/CMS/SingleTopHiggsGeneration13TeV>,
 1260 last accessed on 16.01.2018.

- 1261 [52] CMS Collaboration, “SM Higgs production cross sections at $\sqrt{s} = 13$ TeV.”
 1262 <https://twiki.cern.ch/twiki/bin/view/LHCPhysics/CERNYellowReportPageAt13TeV>,
 1263 last accessed on 16.01.2018.
- 1264 [53] S. Dawson, The effective W approximation, Nucl. Phys. B 249 (1985) 42.
- 1265 [54] S. Biswas, E. Gabrielli and B. Mele, JHEP 1301 (2013) 088 [arXiv:1211.0499
 1266 [hep-ph]].
- 1267 [55] CMS Collaboration, “Search for the associated production of a Higgs boson
 1268 with a single top quark in proton-proton collisions at $\sqrt{s} = 8$ TeV”, JHEP 06
 1269 (2016) 177, doi:10.1007/JHEP06(2016)177, arXiv:1509.08159.
- 1270 [56] B. Stieger, C. Jorda Lope et al., “Search for Associated Production of a Single
 1271 Top Quark and a Higgs Boson in Leptonic Channels”, CMS Analysis Note CMS
 1272 AN-14-140, 2014.
- 1273 [57] M. Peruzzi, C. Mueller, B. Stieger et al., “Search for ttH in multilepton final
 1274 states at $\sqrt{s} = 13$ TeV”, CMS Analysis Note CMS AN-16-211, 2016.
- 1275 [58] CMS Collaboration, “Search for H to bbar in association with a single top quark
 1276 as a test of Higgs boson couplings at $\sqrt{s} = 13$ TeV”, CMS Physics Analysis
 1277 Summary CMS-PAS-HIG-16-019, 2016.
- 1278 [59] B. Maier, “SingleTopHiggProduction13TeV”, February, 2016.
 1279 <https://twiki.cern.ch/twiki/bin/viewauth/CMS/SingleTopHiggsGeneration13TeV>.
- 1280 [60] M. Peruzzi, F. Romeo, B. Stieger et al., “Search for ttH in multilepton final
 1281 states at $\sqrt{s} = 13$ TeV”, CMS Analysis Note CMS AN-17-029, 2017.
- 1282 [61] B. WG, “BtagRecommendation80XReReco”, February, 2017.
 1283 <https://twiki.cern.ch/twiki/bin/view/CMS/BtagRecommendation80XReReco>.